Phase separation of Treacle is indispensable for ribosomal transcription and DNA repair

Artem K. Velichko[1,2,3], Anastasia P. Kovina[1], Artem V. Luzhin[1,2], Nadezhda V. Petrova[1], Dmitry A. Deriglazov[1], Eugene P. Kazakov[4], Igor I. Kireev[4], Victoria O. Shender[5,6], Georgij P. Arapidi[5,6], Sergey V. Razin[1,7], and Omar L. Kantidze[1,8,*]

[1]Department of Cellular Genomics, Institute of Gene Biology RAS, Moscow, Russia

[2]Center for Precision Genome Editing and Genetic Technologies for Biomedicine, Institute of Gene Biology RAS, Moscow, Russia

[3]Institute for Translational Medicine and Biotechnology, Sechenov First Moscow State Medical University, Moscow, Russia

[4]A.N. Belozersky Institute of Physico-Chemical Biology, Lomonosov Moscow State University, Moscow, Russia

[5]Shemyakin-Ovchinnikov Institute of Bioorganic Chemistry of the Russian Academy of Sciences, Moscow, Russia

[6] Lopukhin Federal Research and Clinical Center of Physical-Chemical Medicine of Federal Medical Biological Agency; Moscow, Russia

[7]Biological Faculty, Lomonosov Moscow State University, Moscow, Russia

[8]Quantori LLC, Cambridge, MA, USA

[*]Corresponding author: Omar Kantidze (kantidze@gmail.com)

Short title: Phase separation of Treacle promotes rDNA transcription and repair

Abstract

It is known that major nuclear processes occur differently in the nucleolus when compared to the remainder of the nucleus. This variation could be associated with the nature of the nucleolus, which is considered a multi-component liquid environment. Among the numerous nucleolar proteins, Treacle holds a special place due to a wealth of experimental evidence highlighting its significance for transcription as well as DNA repair in the nucleolus. However, it remains unclear how Treacle exerts its multifaceted influence on nucleolar processes from a mechanistic perspective. In this study, we demonstrate that Treacle can undergo phase separation in living cells and characterize the structural basis of its condensation and generation of cooperative Treacle-TOPBP1 liquid assemblies. Our data clearly show that the phase separation of Treacle serves a key role in ribosomal DNA transcription and DNA repair. In these processes, Treacle biomolecular condensates serve as a platform for attracting and retaining transcription machinery (UBF1, Pol I) or repair factors (TOPBP1, ATR, and others) on ribosomal genes. Moreover, Treacle and TOPBP1 can form cooperative nuclear biomolecular condensates in the absence of DNA damage. These damage-independent Treacle-TOPBP1 liquid droplets act as fully functional molecular platforms for DNA damage response activation. Our data indicate that by forming biomolecular condensates, Treacle can facilitate intracellular processes and target them to the required intranuclear locations.

Introduction

Applying polymer chemistry principles to biological molecules has significantly widened our understanding of membraneless compartments' functioning (Mehta & Zhang, 2022, Mittag & Pappu, 2022). Multiple weak, cooperative, and dynamic interactions underlie the assembly of these self-organized structures, termed biomolecular condensates. Mechanistically, liquid–liquid phase separation (LLPS)—a process of de-mixing that yields a condensed protein-enriched phase and a dilute phase—can mediate the self-assembly of biomolecular condensates. Phase separation is mainly a characteristic of multivalent or intrinsically disordered proteins (Banani *et al*, 2017, Shin *et al*, 2017). Biomolecular condensates serve as functional hubs in diverse cellular processes such as transcription (Sabari *et al*, 2020), microtubule nucleation (Woodruff *et al*, 2017), and adaptive stress response (Franzmann & Alberti, 2019). Moreover, a large and complex subnuclear compartment such as the nucleolus can also be considered a multicomponent and multilayered biomolecular condensate (Lafontaine *et al*, 2021). The nucleolus is formed around arrays of ribosomal gene repeats (rDNA), which are transcribed by RNA polymerase I (Pol I) to produce pre-ribosomal RNA (Cerqueira & Lemos, 2019). In the nucleolus, RNAs and hundreds of different proteins are segregated into three immiscible liquid phases: the fibrillar center (FC), which is the inner layer that contains the machinery for ribosomal RNA gene (rDNA) transcription through RNA polymerase I (Pol I); the dense fibrillar component (DFC), which is the intermediate layer that is rich in fibrillarin; the granular component (GC), which is the outer layer that is rich in nucleophosmin (NPM1). Although purified fibrillarin and NPM1 can separate into two distinct phases *in vitro* to create the droplet compartments of DFC and GC, respectively, the nature of the FC droplet compartment remains unclear (Feric *et al*, 2016). By examining the behavior of the FC in living cells, it has been proposed that the FC's organization is a result of phase separation (Falahati *et al*, 2016, Falahati & Wieschaus, 2017). Furthermore, several studies have shown that the FC components relocate to the periphery of the nucleolus and aggregate to form large structures

called nucleolar caps when RNA Pol I transcription is inhibited by using actinomycin D (AMD) or genotoxic drugs (Harding *et al*, 2015, Korsholm *et al*, 2019, Reynolds *et al*, 1964). This transformation process exhibits similarities to the fusion of liquid droplets. Treacle is the main molecule present in the FC, and it has both transcription-dependent and -independent(Gal *et al*, 2022)). Its role in ribosome biogenesis is well-documented since it assists in the transcription and processing of rRNA (Gonzales *et al*, 2005, Lin & Yeh, 2009, Valdez *et al*, 2004). Furthermore, it is the primary regulator of DNA damage response (DDR) in the nucleolus (Ciccia *et al*, 2014, Korsholm *et al*, 2019, Larsen *et al*, 2014, Mooser *et al*, 2020). Treacle serves a crucial role in the regulation of rDNA transcription, as well as in recruiting repair factors to rDNA damage caused by IPpoI-induced breaks, replication stress, or R-loop formation (Mooser *et al*, 2020, Velichko *et al*, 2021, Velichko *et al*, 2019). It acts as a nucleolar hub with both transcriptional and repair functions. The reason for its multifunctionality can be attributed to its possible ability to undergo phase separation and engage in multivalent interactions. Protein structure predictors indicate that Treacle is one of the most intrinsically disordered proteins. In addition, Treacle's partners in transcription and DNA repair (Pol I and TOPBP1, respectively) also utilize condensation as a functioning mechanism (Frattini *et al*, 2021, Ide *et al*, 2020). Pol I can inhibit the transcription of ribosomal genes by undergoing phase separation, while TOPBP1 condensation can activate the ATR signaling pathway (Frattini *et al*, 2021, Ide *et al*, 2020). However, it is currently unknown whether Treacle itself can undergo phase separation. To fill this knowledge gap, we investigated its potential for phase separation.

In this study, we demonstrate for the first time that Treacle can undergo phase separation *in vivo*. Moreover, we characterize in detail the structural basis of TOPBP1 condensation. Our findings indicate that phase separation is crucial for Treacle to facilitate the transcription of ribosomal genes. This is accomplished by ensuring the proper recruitment, retention, and dynamics of both Treacle and its partners involved in ribosomal gene transcription. Moreover, we show the importance of the LLPS properties of Treacle for forming cooperative condensates with TOPBP1 and maintaining

rDNA repair. Using an artificial droplet model of overexpressed Treacle and TOPBP1, we have established that these proteins bind constantly and that the ratio of TOPBP1 to Treacle in the cooperative condensate is critical in regulating DDR activation. The ATR-dependent TOPBP1 oligomerization results in an increase in the proportion of Treacle-bound TOPBP1, which attracts other repair factors and triggers DDR, even in the absence of physical DNA damage. Therefore, the cooperative Treacle-TOPBP1 condensate generates a novel intranucleolar phase with a high affinity for other repair proteins. Using the examples of different types of genotoxic stress, we show that Treacle–TOPBP1 biomolecular condensate formation in the nucleolus is critical to the efficient repair of different types of rDNA damage. Our study demonstrates that Treacle's ability to undergo phase separation is essential for integrating its functions of ensuring ribosomal gene transcription and preserving rDNA integrity.

Results

Treacle drives the formation of biomolecular condensates

According to protein structure predictors (e.g., AlphaFold, IUPred2, PONDR, FuzDrop), Treacle is one of the most intrinsically disordered proteins (Fig. S1A). To study the capacity of Treacle to self-organize into biomolecular condensates, we first fused Treacle to FusionRed (a fluorescent protein that lacks a tendency to self-dimerize) and to the *Arabidopsis thaliana* cryptochrome 2 (Cry2) protein, which undergoes oligomerization upon exposure to blue light, thus seeding the formation of biomolecular condensates (so-called, “optoDroplets”) (Shin *et al*, 2017). We expressed this opto–Treacle chimeric protein in human HeLa cells and found that without blue light illumination, it only formed foci in nucleoli, reflecting Treacle's natural property of occupying FCs (Fig. 1A; for controls, see Fig. S1B and S1C). Upon exposure of these cells to blue light, opto–Treacle formed multiple small-sized foci throughout the nucleoplasm (Fig. 1A). For an in-depth study, it was more convenient to use Treacle condensates that do not require light-induced oligomerization. Therefore, we assessed whether Treacle could form biomolecular condensates when overexpressed as a fusion

with Katushka, a bright far-red fluorescent protein (Shcherbo *et al*, 2007). We found that at a low level of Treacle–Katushka expression, it only forms foci in nucleoli, reflecting the occupation of FCs (Fig. 2B). However, as the expression level increased, it began to form large extranucleolar spherical structures in the nucleoplasm (Fig. 1B). Both intranucleolar and extranucleolar Treacle–Katushka foci—induced by low and high levels of fusion protein expression, respectively—had a spherical shape with an aspect ratio close to one (Fig. 1C). This suggests that Treacle condensates may be subjected to surface tension. To confirm the internal homogeneity of Treacle droplets, we conducted transmission electron microscopy imaging. The images showed circular droplet-like structures that mostly appeared to contain homogenous protein content without any electron-dense or -light regions inside the droplets (Fig. S1D).

One of the characteristics of liquid droplets is their capacity to merge with each other. Our findings indicate that during actinomycin D-induced rDNA transcriptional repression, nucleolar caps form due to the fusion of intranucleolar Treacle–Katushka foci (Fig. 1D, Movie S1). Prolonged live-cell imaging demonstrated that the extranucleolar biomolecular condensates of Treacle–Katushka also frequently fuse, indicating their ability to undergo dynamic clustering (Fig. 1E, Movie S2).

Liquid condensates are characterized by a high rate of molecular exchange within them, which is often demonstrated using the fluorescence recovery after photobleaching (FRAP) method. It is technically impossible to bleach a part of an FC due to its small size. However, even when Treacle is bleached within a whole FC, the half-recovery time is approximately 1.5–2 minutes, which reflects a relatively rapid exchange. Interestingly, in nucleolar caps induced by actinomycin D, the dynamics of Treacle are greatly increased since the half-recovery time decreases to several tens of seconds (Fig. 1F). Treacle in extranucleolar droplets induced by its overexpression has a similar dynamic behavior (Fig. 1G). Although this recovery is slower than the exchange rate of some well-known liquid condensates, it still indicates the exceptional mobility of Treacle condensates. These data also suggest that the transformation of FCs into nucleolar caps upon

transcriptional inhibition causes Treacle to transition to a more liquid-like behavior, which is very similar to the previously described behavior of Pol I (Ide *et al*, 2020).

Unexpectedly, opto–Treacle droplets and the droplets of overexpressed Treacle–Katushka demonstrated resistance to 1,6-hexanediol, sodium chloride, and heat stress, indicating that they did not rely on electrostatic or weak hydrophobic interactions (Fig. S1E–G). Altogether, these findings suggest that although Treacle has LLPS properties, the resulting biomolecular condensates exhibit both liquid- and gel-like behavior. While Treacle assemblies are mobile and possess the main characteristics of LLPS-mediated structures, they are slightly more stable than many known membraneless compartments.

Phosphorylation of Treacle is essential for assembling biomolecular condensates

Our next aim was to investigate the structural features of the Treacle protein that contribute to its capacity for creating biomolecular condensates. Although Treacle is a low-complexity protein, it consists of three functional domains: the N-terminal and C-terminal domains, which are divided by a central region containing repeated sequence motifs (Fig. 2A). To identify the domains contributing to its phase separation, we created several deletion mutants of Treacle fused with Katushka and overexpressed them in HeLa cells (Fig. 2A). Deletion mutants lacking both N- and C-terminal domains (D1,3) were unable to enter the nucleus and generate biomolecular condensates. Mutants lacking either the C-terminal domain (D3) or both the C-terminal and central domains (D2,3) were evenly distributed throughout the nucleus and unable to form liquid droplets inside or outside the nucleolus (Fig. 2A–C). The C-terminal domain (D1,2) was present in the nucleolus but did not accumulate in clearly distinguishable fibrillar centers. Although the central domain (D1,3) did not enter the nucleus, its inability to generate droplets in combination with the N-terminal domain (D2,3) suggests that it cannot form droplets on its own. Droplet formation like that observed in full-length Treacle expression was only observed in the form of Treacle protein

truncated at the N-terminus (D1), indicating that the central and C-terminal domains of Treacle are likely to serve a major role in droplet formation (Fig. 2A–C).

Endogenous Treacle is known to be intensely phosphorylated, especially in the central domain (Mooser *et al*, 2020). In the next set of experiments, we aimed to determine whether overexpressed Treacle undergoes phosphorylation and whether such phosphorylation is necessary for its condensation. First, we performed LC-MS/MS analysis of the phosphoproteome of HeLa cells overexpressing Treacle–Katushka. We detected many sites within the Treacle protein sequence that had undergone phosphorylation (Fig. 2D and Supplementary Table 6). Among these sites, 47 were identified as consensus sequences for casein kinase 2 (CK2), while only 3 sites were for PIKKs (ATM/ATR/DNA-PK; Fig. 3D). We treated Treacle–Katushka-overexpressing HeLa cells with wortmannin (an inhibitor of ATM, ATR, and DNA-PK) or CK2 inhibitor CX-4945 to eliminate the corresponding Treacle phosphorylation patterns in order to determine whether phosphorylation is necessary for Treacle condensate formation. Whereas the formation of Treacle biomolecular condensates was not affected by the pharmacological suppression of ATR, ATM, and DNA-PK, Treacle–Katushka condensation was suppressed by CK2 inhibition (Fig. S2A). To confirm the importance of CK2-dependent phosphorylation for Treacle condensation, we created Treacle–Katushka mutants (Ph-mut) that lacked CK2 phosphorylation residues in the central domain of Treacle (notably, CK2 phosphorylation sites in the N- and C-terminal domains were intentionally left intact). Similar to the Treacle D1,2 mutant completely lacking N-terminal and central domains, the Treacle Ph-mut was found to accumulate in the nucleolus without forming extranucleolar droplets—even at high expression levels (Fig. 3E). Super-resolution microscopy (3D-SIM) analysis demonstrated that both Treacle D1,2 and Ph-mutants were unable to form nucleolar fibrillar centers (Fig. 2F). These findings suggest that the presence of C-terminal and central domains, as well as CK2-dependent phosphorylation of the latter, are crucial for the formation of both intra- and extranucleolar Treacle biomolecular condensates.

Treacle biomolecular condensates promote ribosomal transcription

Treacle is present in the fibrillar centers of the nucleolus, where it interacts with UBF1 proteins and RNA polymerase I (Pol I) to control the transcription and processing of ribosomal RNA (Lin & Yeh, 2009, Valdez *et al*, 2004). Thus, we aimed to explore the role of Treacle condensates in the organization of the nucleolus structure and the transcription of rRNA. We observed that both intranucleolar and extranucleolar Treacle–Katushka foci, which were generated by low and high levels of fusion protein expression, respectively, co-localized with UBF1 and Pol I subunit RPA194 (Fig. 3A). Interestingly, our findings showed that treating the cells with high salt concentrations resulted in the release of UBF1 and RPA194 from a Treacle droplet (Fig. 3B). Our results indicate two main conclusions: (i) the presence of partner proteins, such as UBF1 and Pol I, may not be essential for maintaining Treacle droplets; (ii) Treacle serves as a molecular platform for retaining proteins involved in rDNA transcription. It seems that Treacle droplets may concentrate rDNA transcription factors at ribosomal genes, ultimately promoting rRNA synthesis. To verify this, we overexpressed Treacle's deletion mutants lacking the capacity to form biomolecular condensates (D1,2 or Ph-mutants) in Treacle-knockout cells. We then evaluated the rRNA transcription level and examined the occupation of the rDNA promoter by Treacle mutants, UBF1, and RPA194. As a control, we overexpressed the full-length Treacle or D1 mutant, both of which retained the ability to form droplets.

In contrast to the full-length Treacle and the D1 mutant, both D1,2, and Ph-mutants decreased the efficiency of rDNA transcription (Fig. 3C). Interestingly, the mechanism of transcriptional inhibition for D1 and Ph-mutants was different. Compared to full-length Treacle and the D1 mutant, the D1,2 mutant had a significantly weaker binding to the promoter of ribosomal genes and also reduced its occupancy by UBF1 and RPA194. At the same time, the Ph-mutant exhibited stronger binding to the promoter and enhanced the binding of UBF1 and RPA194 (Fig.

3C). We hypothesized that the loss of functionality in the D1,2 mutant might be related to its fundamental inability to undergo phase separation, whereas full-length but unphosphorylated Treacle loses functionality due to its transition into a more aggregated state with low protein dynamics.

Overall, these results suggest that Treacle's biomolecular condensates recruit nucleolar transcription components to the promotors of ribosomal genes and provide rRNA transcription.

The interaction between Treacle and TOPBP1 depends on the formation of Treacle biomolecular condensates

Previous studies have shown that the DNA repair protein TOPBP1 is a known interaction partner of Treacle (Mooser *et al*, 2020, Velichko *et al*, 2021). Our next aim was to explore whether the interaction between Treacle and TOPBP1 is facilitated by the ability of Treacle to form condensates, as well as to identify the key structural elements of Treacle that are involved in this interaction. We initially investigated whether endogenous TOPBP1 could be recruited to nuclear Treacle condensates induced by the overexpression of Treacle–Katushka protein or light stimulation of opto–Treacle. We observed not only the co-localization of TOPBP1 with opto–Treacle and Treacle–Katushka (Fig. 4A–B) but also the physical interaction between TOPBP1 and Treacle on the surface of these biomolecular condensates, as shown by using a proximity ligation assay (PLA) (Fig. 4C). Moreover, we demonstrated that the presence of TOPBP1 does not affect the ability of Treacle to form droplets, even when the quantity of endogenous TOPBP1 was reduced via RNA interference (Fig. S4A).

To investigate the impact of weak electrostatic and hydrophobic forces on the interaction between Treacle and TOPBP1, we subjected HeLa cells overexpressing Treacle to hyperosmotic stress or treated them with 10% 1,6-hexanediol. Using indirect immunofluorescence, we found that only hyperosmotic treatment induced the release of TOPBP1 from Treacle droplets, while 1,6-hexanediol did not affect these combined Treacle–TOPBP1 condensates (Fig. S4C–D).

In summary, within the Treacle-TOPBP1 biomolecular condensates, Treacle serves as a stable core component, while TOPBP1 displays a high degree of mobility. We determined that the primary driving force behind the interaction between Treacle and TOPBP1 in the condensate is electrostatic interaction.

Next, we investigated the structural characteristics of Treacle that facilitate its interaction with TOPBP1 and the formation of a heterologous Treacle-TOPBP1 droplet. Mooser et al. reported that the interaction between TOPBP1 and Treacle occurs via phosphoserines 1190/1191 in a conserved acidic sequence motif (Mooser *et al*, 2020). To investigate the importance of these serines for the interaction, we generated a mutated version of Treacle–Katushka with deleted serines 1190/1191 and overexpressed it in HeLa cells. We observed that although this mutant could efficiently form liquid condensates, it could not interact with TOPBP1 (Fig. 4D–F). Notably, the SSEDD motif containing the 1190/1191 serines shares similarity with the consensus sequence for CK2. Phosphoproteomic analysis of the overexpressed wild-type Treacle indicated that the 1190/1191 serines were significantly phosphorylated. Based on these observations, we proposed that CK2 might regulate the phosphorylation of this site in Treacle, thereby modulating the interaction with TOPBP1. To confirm this, we utilized CX-4945 (an inhibitor of CK2) and observed that it prevented TOPBP1 from localizing in Treacle droplets, whereas wortmannin had no effect (Fig. 4G–I). We also discovered that Treacle deletion mutants (D1,2 and Ph-mutant), which lacked the capacity for phase separation despite having intact 1190/1191 serines, were also incapable of localizing with TOPBP1 (Fig. 4J–K). Thus, two conditions must be met for Treacle to interact with TOPBP1. First, Treacle must be able to create biomolecular condensates. Second, serines 1190/1191 must be phosphorylated by CK2.

The level of TOPBP1 in Treacle condensates can regulate DDR without physical DNA damage

TOPBP1 constitutively binds to Treacle condensates under normal physiological conditions (this paper and (Mooser *et al*, 2020)). However, to activate DDR in ribosomal genes during genotoxic

stress, an elevated amount of TOPBP1 associated with Treacle is required. Our hypothesis suggests that the regulation of DDR is determined by the ratio of Treacle to TOPBP1 within the heterologous condensate. We sought to test this hypothesis by utilizing synthetic condensates consisting of overexpressed Treacle and TOPBP1 proteins. We expressed Treacle–GFP and TOPBP1-FusionRed separately in HeLa cells or co-expressed them in different ratios and subsequently examined the generation of phosphorylated H2AX foci. Biomolecular condensates of overexpressed Treacle that only contained endogenous TOPBP1 did not exhibit H2AX phosphorylation (H2AX-negative; Fig.5A). Using indirect fluorescence microscopy and PLA, we verified that as the level of TOPBP1 expression increased, its localization and interaction with Treacle condensates were enhanced (Fig.5A–C). Notably, as the concentration of TOPBP1 within the droplets increased, we observed the initiation of histone H2AX phosphorylation on the surface of the droplets (H2AX-positive; Fig. 5A–C). When only TOPBP1-FusionRed was overexpressed, the formation of Treacle-TOPBP1 droplets occurred solely due to endogenous Treacle but also resulted in an H2AX-positive outcome (Fig. 5A). To differentiate between Treacle condensates with low and high TOPBP1 content, we will henceforth refer to those with low TOPBP1 content as “TT droplets” (TOPBP1-Treacle), and those with high TOPBP1 content as “mTT droplets” (multiple TOPBP1-Treacle). Notably, mTT droplets retained their liquid state similar to the TT droplets, thus displaying efficient fusion (Fig. S5A), the high mobility of both Treacle and TOPBP1 (Fig. S5B), and a comparable response to hyperosmotic treatment and 1,6-hexanediol (Fig. S5C).

rDNA FISH analysis revealed that certain TT and mTT droplets remained associated with ribosomal genes (Fig. S5D). Subsequent ChIP-qPCR and RT-PCR analyses confirmed that mTT droplets induced the phosphorylation of H2AX in ribosomal genes (Fig. 5D) and led to the repression of rDNA transcription (Fig. 5E). Collectively, these findings demonstrate that the generation of mTT droplets triggers DDR in ribosomal DNA. We also examined the spatial distribution of several DNA repair factors at mTT droplets and found that most of these DDR proteins—including phospho-ATM, phospho-ATR, 53BP1, BRCA1, MDC1, and Nbs1—

accumulated at the surface of mTT droplets (Fig. 5F). However, other DDR proteins (ETAA1, XRCC1, and PARP1) were not recruited to mTT droplets (Fig. S5E). The observation that DDR proteins exhibiting LLPS properties (53BP1 and PARP1) were recruited differently to mTT droplets suggests that the recruitment of DNA repair factors is regulated by protein-protein interactions and the physicochemical properties of Treacle–TOPBP1 condensates.

We conducted further experiments to determine whether the formation of mTT droplets resulted in physical DNA damage, which could potentially trigger the accumulation of DNA repair proteins within the droplets. First, we induced the formation of TT droplets by expressing Treacle–GFP and mTT droplets by co-expressing Treacle–GFP and TOPBP1–FP in HeLa cells. We then sorted the cells into two populations (one expressing TT droplets and the other expressing mTT droplets) and performed a neutral comet assay on each population. The results showed that neither the formation of TT droplets nor mTT droplets induced double-strand breaks (DSBs) (Fig. S5F). Additionally, to confirm that mTT droplet formation did not stimulate DNA damage, we used the TdT-IP approach to analyze the formation of DNA lesions specifically in ribosomal repeats. We found that neither the formation of TT droplets nor mTT droplets induced DNA damage in ribosomal genes (Fig. 5G).

Thus, the formation of mTT droplets triggers the same DDR pathway observed in the case of genotoxic damage to rDNA, making it a useful model for investigating the DNA damage response in ribosomal genes. Our findings indicate that an increased concentration of TOPBP1 within a Treacle condensate is sufficient to activate a complete DDR response without causing physical DNA damage. Additionally, the activation of DDR is not limited to ribosomal genes but can occur anywhere in the nucleus where an mTT droplet is present.

The activation of DDR occurs as a result of the ATR-dependent oligomerization of TOPBP1 within Treacle biomolecular condensates

To explore the mechanisms responsible for TOPBP1-induced DDR activation within mTT droplets, we addressed three primary questions: (i) whether DDR activation during mTT droplet formation is triggered by the binding of TOPBP1 to Treacle or simply by the overexpression of TOPBP1; (ii) how PIKKs are involved in TOPBP1-mediated DDR activation in mTT droplets; (iii) whether the increase in the proportion of Treacle-associated TOPBP1 in mTT droplets is a regulated or passive process driven solely by TOPBP1 overexpression. ChIP-qPCR analyses demonstrated that an elevation of TOPBP1 expression leads to an increase in H2AX phosphorylation not only in ribosomal genes but also in other genomic regions, such as the GAPDH gene or Alu repeats (Fig. 5D). Based on this discovery, we concluded that DDR activation was not a result of direct interaction between Treacle and TOPBP1. Instead, the overexpression of TOPBP1 alone could activate DDR, with Treacle droplets functioning more as a framework for the capture of TOPBP1 and the localization of DDR. To confirm this further, we overexpressed TOPBP1-FusionRed in cells where Treacle was downregulated and then evaluated the level of DDR in various genomic regions, including ribosomal genes, the GAPDH gene, and Alu repeats. In Treacle-knockdown cells, TOPBP1-FusionRed could not form droplets; instead, it had a uniform pan-nuclear distribution. It induced pan-nuclear histone H2AX phosphorylation that was no longer localized in ribosomal genes but increased in the GAPDH gene and Alu repeats (Fig. 6A, C). Simultaneously, rDNA transcription was no longer repressed (Fig. 6B). We obtained similar results when we co-expressed TOPBP1-Flag with Treacle mutants that could not interact with TOPBP1, such as Treacle–GFP ph-mut, Treacle–GFP D1,2, and Treacle–GFP S1190/1191 del (Fig. S6A–B). Our findings indicate that when TOPBP1 is overexpressed but cannot integrate into Treacle droplets, it randomly activates DDR throughout the genome. On the other hand, when TOPBP1 is sequestered in mTT droplets, it triggers a DDR that specifically targets the genomic regions where mTT droplets are located, particularly in ribosomal genes.

We performed an inhibitory assay to identify which of the PIKKs are involved in DDR control during mTT droplet formation. We found that inhibiting ATR kinase led to a complete

blockade of DDR, whereas inhibiting ATM or DNA-PK did not have this effect. When we treated cells with VE-821 (ATR inhibitor), we observed that mTT droplets became H2AX-negative (Fig. 6D), H2AX phosphorylation was inhibited in both rDNA and Alu repeats (Fig. 6E), and ribosomal gene transcription repression was prevented (Fig. 6F).

We further supported our findings by performing chromatin immunoprecipitation, which demonstrated a clear connection between DDR activation in ribosomal genes and the presence of the active form of ATR kinase in these regions (Fig. 6G). PLA analysis (Fig. 6H) revealed that inhibiting ATR led to a decrease in the binding of TOPBP1 to Treacle, which caused mTT droplets to convert into TT droplets. These findings suggest that the increase in the proportion of TOPBP1 in Treacle droplets during mTT droplet formation is not solely a passive process but is also controlled by ATR. However, the precise mechanism underlying this regulation is still not well understood. Our observations indicate that even with overexpression, TOPBP1 did not localize to the condensates of Treacle that lacked serines 1190/1191 (Fig. S6A). We also utilized the PLA technique and discovered that inhibiting ATR kinase alone decreased the interaction between TOPBP1 and Treacle in mTT droplets to the constitutive level observed in TT droplets. Only when CK2 kinase was inhibited or serines 1190/1191 were deleted from Treacle was the interaction completely blocked (Fig. 6H).

Based on our findings, it appears that phospho-serines 1190/1191 are the sole sites of Treacle interaction for both constitutive and inducible TOPBP1. Since these serines are consensus sites for CK2 rather than ATR, other parts of TOPBP1 are likely drawn to the Treacle droplet not by ATR-mediated modifications of Treacle, but by the ATR-dependent modification of TOPBP1 itself. To directly investigate this hypothesis, we generated two TOPBP1-flag deletion mutants. The first mutant had a deletion of the BRCT 7/8 domains, which cannot oligomerize but can activate ATR. The second mutant had a deletion of the AAD domain, which cannot activate the ATR kinase but can support oligomerization. We fused both of these mutants with the FKBP F36V tag, which allows for dimerization to be induced by the addition of the rapamycin analog AP20187 (Fig. 6I).

We co-expressed these mutants with Treacle–GFP and evaluated the level of DDR and the extent of protein interaction in the droplets before and after the AP20187-induced dimerization of TOPBP1. In the absence of AP20187, both TOPBP1 mutants were localized in Treacle droplets but failed to trigger DDR (Fig. 6I–K). Upon the addition of AP20187, only the TOPBP1-BRCT7/8 mutant—and not the TOPBP1-AAD mutant—could form H2AX-positive droplets with Treacle and activate DDR in ribosomal genes (Fig. 6I–K). Surprisingly, we observed that both TOPBP1 mutants increased their interactions with Treacle upon the addition of AP20187, as demonstrated by PLA (Fig. 6L).

These results suggest that the ATR-independent recruitment of TOPBP1 in Treacle droplets occurs upon the forced dimerization of TOPBP1, while ATR activity is limited only by the activation of DDR. Conversely, the overexpression of wild-type TOPBP1 results in the ATR-mediated formation of TOPBP1 oligomers, which concentrate in Treacle droplets. In both the TT droplet monomers and the mTT droplet oligomers, TOPBP1 binds to Treacle due to the CK2-dependent phosphorylation of serines 1190/1191. Our findings suggest that the forced dimerization of TOPBP1 leads to its recruitment to Treacle droplets independently of ATR, where ATR activity is only required for DDR activation. In contrast, the overexpression of wild-type TOPBP1 results in the ATR-dependent formation of TOPBP1 oligomers that are concentrated in Treacle droplets. Both the TOPBP1 monomers in TT droplets and oligomers in mTT droplets interact with Treacle through the phosphorylation of serines 1190/1191 by CK2.

Treacle–TOPBP1 condensate formation is essential for DDR induction in ribosomal genes under genotoxic stress

We decided to evaluate the applicability of the mechanisms involved in the generation and function of artificial mTT droplets in regard to endogenous TOPBP1 and Treacle under the conditions of genotoxic stress. To induce rDNA damage, we employed three widely used chemotherapeutics: i) camptothecin (CPT), an inhibitor of topoisomerase I that introduces single-stranded DNA breaks (SSBs) (Talukdar *et al*, 2022); ii) etoposide (VP16), a topoisomerase II poison inducing DSBs (Bax

et al, 2019); iii) bleomycin (Bleo), a radiomimetic that results in clustered DNA damage (Regulus *et al*, 2007). In all cases, such DNA damage stimulated the rapid accumulation of the TOPBP1 repair protein within the nucleolus, as shown by indirect fluorescence microscopy (Fig. 7A–C).

TOPBP1 and Treacle co-localized in the nucleoli in response to DNA damage (Figs. 7C and S7A). Furthermore, ChIP-seq analysis revealed that TOPBP1 binding to ribosomal genes was significantly increased following DNA damage, and the pattern of TOPBP1 distribution was identical to that of Treacle (Fig. 7D). In addition, the PLA analysis conducted after DNA damage induction provided evidence of a physical association between TOPBP1 and Treacle (Figs. 7E and S7B). The observations of TOPBP1 occupancy on ribosomal genes in undamaged cells and interaction between the two proteins suggest that even under normal physiological conditions, TOPBP1 and Treacle interact with each other, while DNA damage induction simply facilitates this association.

We utilized indirect immunofluorescence microscopy and chromatin immunoprecipitation to demonstrate that, similarly to mTT droplets, the etoposide-induced interaction between endogenous TOPBP1 and Treacle is electrostatic in nature and completely depends on the activities of ATP and CK2 kinases (Figs. 7F and S7D). Additionally, we demonstrated that when endogenous Treacle was knocked down, the occupancy of rDNA by TOPBP1 during genotoxic stress could be restored by the overexpression of either a full-length Treacle or its D1 mutant (Figs. 7G–H and S7E). However, this was not the case with a Treacle mutant that lacked serines 1190/1191 or D1,2 and Ph-mutants that could not form biomolecular condensates (Figs. 7G-H and S7E). We then investigated whether the interaction between Treacle and TOPBP1 serves a role in activating DDR in ribosomal genes and whether this DDR is facilitated by the ability of Treacle to form condensates. The interaction between Treacle and TOPBP1 resulted in the suppression of transcription of ribosomal genes and the formation of nucleolar caps caused by the fusion of Treacle–Katushka foci in the nucleolus when VP16 was administered to the cells (Fig. 7I–J).

Using ChIP-qPCR with antibodies against the panel of DNA repair proteins and phosphoproteins in Treacle-depleted cells, we also observed that the activation of ATM/ATR kinases, phosphorylation of histone H2AX, and the recruitment of repair factors (e.g., 53BP1 and BRCA1) to the promoter of ribosomal genes under genotoxic stress could be compensated by overexpression of a full-length Treacle but not a D1,2 or a Ph-mutant lacking the ability to phase separate (Figs. 7K and S7F). Ultimately, we determined that the lack of either Treacle or TOPBP1 had a negative impact on the repair of DNA lesions in rDNA induced by VP16, as determined through TdT-IP experiments with cells depleted of Treacle or TOPBP1 (Fig. 7L).

These results demonstrate that regardless of the type of rDNA lesion, Treacle and TOPBP1 are essential for efficient nucleolar DDR and repair. Together with our previous findings on the involvement of these factors in the nucleolar replication stress response (Velichko *et al*, 2021), these results suggest that Treacle-TOPBP1 cooperative condensates may function as a universal molecular platform for nucleolar DDR.

Discussion

The nucleolus is a multi-component phase condensate primarily responsible for ribosome biogenesis (Lafontaine *et al*, 2021). As the transcribed rRNA undergoes processing and gets integrated into forming ribosomes, it moves from FCs to the DFC and eventually to the GC (Lafontaine *et al*, 2021). Each nucleolar compartment creates a distinct environment by demixing into a separate phase of a protein which acts as a constitutive component of that specific compartment and then recruiting client proteins to this separate phase. Nucleolin and nucleophosmin are the constitutive components of DFC and GC, respectively (Feric *et al*, 2016). However, the identification of the protein playing a similar role in FCs remains a subject of debate. Our results, combined with the observations made by other researchers, suggest that the nucleolar phosphoprotein Treacle, encoded by the TCOF1 gene, probably plays this role.

The presence of Treacle in FCs has been confirmed through multiple studies (Gal *et al*, 2022, Grzanka & Piekielko-Witkowska, 2021, Isaac *et al*, 2000). According to various protein complexity predictors, Treacle is one of the highly intrinsically disordered proteins. In this study, we present experimental evidence that establishes Treacle's ability to undergo LLPS, which elucidates its function as an organizer of nucleolar FCs and a molecular scaffold for various nucleolar processes.

Our experiments revealed that when Treacle is overexpressed in cells, it forms structures that exhibit biophysical properties resembling liquid droplets. Notably, we discovered that the ability of Treacle to undergo LLPS is regulated by CK2-dependent phosphorylation. By examining a Treacle mutant lacking CK2 consensus sites within its central domain, we demonstrated that this mutant is incapable of LLPS and fails to form FCs in the nucleolus. However, the exact mechanism by which phosphorylation facilitates the condensation of Treacle remains unclear. Our hypothesis suggests that phosphorylation of positively charged disordered segments in Treacle transforms these segments into polyampholytes, thereby increasing the valency of intrachain and interchain interactions.

An increasing number of studies have reported the function of Treacle in the recruitment and/or retention of different non-nucleolar proteins in nucleoli (Larsen *et al*, 2014, Mooser *et al*, 2020, Velichko *et al*, 2021, Velichko *et al*, 2019). Under normal conditions, Treacle promotes the retention of Pol I and UBF1 in FCs. The retention of RNA pol I and UBF1 within Treacle condensate appears to be facilitated by electrostatic interactions, as both proteins can be released from the condensate without disrupting its structure when cells are exposed to high salt concentrations. It is logical to assume that Treacle droplets concentrate rDNA transcription factors at ribosomal genes, thereby facilitating rRNA synthesis. To test this hypothesis, we expressed deletion mutants of Treacle that lack the ability to form biomolecular condensates in Treacle-depleted cells. We found that these mutants could not replace the wild-type Treacle in organizing FCs and maintaining a high level of rRNA synthesis. These findings align with earlier published

data, which demonstrated that Treacle knockdown leads to nucleolus disruption (Park *et al*, 2014), the disintegration of FCs, the release of Pol I, UBF, and NOPP140, as well as repression of rDNA transcription (Lin & Yeh, 2009, Valdez *et al*, 2004).

Being involved in organizing FCs, Treacle integrates various signals and orchestrates responses to these signals. Here we studied the role of Treacle in nucleolar DDR. One of the well-known partners of Treacle is TOPBP1, which is primarily involved in the DNA replication stress-induced activation of ATR (Day *et al*, 2021). The necessity for TOPBP1–Treacle interaction for correct nucleoli-specific DDR and replication stress response was recently reported by our group and that of Manuel Stucki (Mooser *et al*, 2020, Velichko *et al*, 2021). From a structural perspective, TOPBP1 is a multi-BRCT-containing protein (Day *et al*, 2021) that can undergo LLPS-mediated condensation (Frattini *et al*, 2021). Here we showed that to attract TOPBP1, Treacle must be able to form droplets and be serine 1190/1191 phosphorylated. In response to DNA damage, the fraction of TOPBP1 associated with the Treacle droplet increases in an ATR-dependent manner. This does not occur due to the modification of Treacle itself but rather due to TOPBP1 oligomerization controlled by ATR. TOPBP1-dependent DDR in Treacle droplets involves the transcriptional repression of ribosomal genes, as well as the recruitment of various repair proteins. Based on our findings, the accumulation within the Treacle-TOPBP1 droplet primarily involves the direct partners of TOPBP1 (ATM, 53BP1, BRCA1), rather than other repair or droplet-forming proteins (PARP1, ETAA1). Therefore, our data indicate that Treacle functions as a seeding scaffold for generating TOPBP1 biomolecular condensates, while TOPBP1 serves as a scaffold for other repair proteins.

Materials and methods

Cell culture and drug treatment

Human HeLa (ATCC® CCL-2™) and HT1080 cells (ATCC® CCL-121™) were cultured in DMEM (PanEco) supplemented with 10% fetal bovine serum (FBS; HyClone/GE Healthcare) and penicillin/streptomycin. The cells were cultured at 37°C in a conventional humidified CO_2 incubator. DNA damage was induced by the treatment of cells with 100 µM bleomycin (Sigma-Aldrich), 1 µM camptothecin (Sigma-Aldrich), or 90 µM etoposide (Sigma-Aldrich, #E1383) for 30 min or 1 h. I-PpoI nuclear translocation was initiated by incubating the cells with 1 µM 4-hydroxytamoxifen (4-OHT) (Sigma-Aldrich, #T176) for 16 h. For rRNA transcription inhibition, cells were treated with 0,05 µg/ml actinomycin D (Sigma-Aldrich, #A1410) for 3 h. For induction of TOPBP1 oligomerization, transfected cells were incubated with 100 nM AP20187 (Sigma-Aldrich, #SML2838) for 24 h. For CK2 inhibition, the cells were treated with 30 µM CX-4945 (Selleckchem, #S2248) for 6 h. For ATR inhibition, the cells were treated with 15 µM VE-821 (Sigma-Aldrich, #SML1415) for 6 h. To obtain 1,6-hexanediol (HD) -treated cells, HeLa cells were incubated with 5% 1,6-HD (Sigma-Aldrich, #240117) in serum-free medium at 37°C in a humidified atmosphere. To obtain sodium chloride-treated cells, HeLa cells were incubated with 500 mM NaCl in a complete culture medium at 37°C in a humidified atmosphere for 30 min.

Plasmid constructs

For the pFusionRED-Treacle-Cry2 (opto-Treacle) construct, the full-length Treacle was amplified by PCR from cDNA with primer set #1 (Supplementary Table 1) using KAPA High-Fidelity DNA Polymerase (KAPA Biosystems, KE2502). The forward and reverse primers contained XhoI sites. The amplified fragment was inserted into the pFusionRed-C vector (Evrogen, FP411) linearized with XhoI. The Cry2 fragment was amplified by PCR from the plasmid pHR-mCh-Cry2WT (Addgene, #101221) with primer set #2 (Supplementary Table 1) digested with NheI and inserted into pFusionRed-Treacle linearized with NheI using NheI enzyme.

For the pFusionRED-FUS-Cry2 construct, the FUS was amplified by PCR from the plasmid pHR-FUSN-mCh-Cry2WT (Addgene, #101223) with primer set #10 (Supplementary Table 1) using KAPA High-Fidelity DNA Polymerase (KAPA Biosystems, KE2502). The forward and reverse primers contained BspEI and KpnII sites respectively. The amplified fragment was inserted into the pFusionRed-C vector (Evrogen, FP411). The Cry2 fragment was amplified by PCR from the plasmid pHR-mCh-Cry2WT (Addgene, #101221) with primer set #2 (Supplementary Table 1) digested with NheI and inserted into pFusionRed-Treacle using NheI enzyme.

To generate pTreacle-GFP or pTreacle-Katushka constructs, the full-length Treacle was amplified by PCR from cDNA with primer set #3 (Supplementary Table 1) using KAPA High-

Fidelity DNA Polymerase (KAPA Biosystems, KE2502). The forward and reverse primers contained BglII and BamHI sites respectively. The amplified fragment was inserted into the pTurboGFP-C (Evrogen, FP511) or pKatushka2S-C (Evrogen, FP761) vectors using BglII/BamHI restriction/ligation.

To make pTOPBP1-FusionRed construct, the TOPBP1 fragment was generated by PCR amplification with primer set #4 (Supplementary Table 1) from the pcDNA3-LacR-TopBP1 plasmid (Addgene, #31317) and was inserted into either the pFusionRed-C (Evrogen, FP411) vectors linearized with SacII.

For the generation of Treacle deletion mutants, D1; D1,2; D2,3; D1,3; D3 fragments were amplified by PCR from the pTreacle-GFP plasmid with primer set #5, #6, #7, #8, and #9 respectively (Supplementary Table 1). The forward and reverse primers contained BglII and BamHI sites respectively. The amplified fragment was inserted into either the pTurboGFP-C (Evrogen, FP511) or pKatushka2S-C (Evrogen, FP761) vectors using BglII/BamHI restriction/ligation.

To obtain the phospho-mutant of Treacle (Treacle-GFP Ph-mut), a fragment encoding the central domain of Treacle (137-1130 aa) was removed from the pTreacle-GFP plasmid using EcoR1 and HindIII restrictases. This fragment was then replaced with a synthetic sequence encoding the same amino acid sequence with deletions of 71 serines at the CK2 kinase consensus sites (see Supplementary Table 5).

For the pTreacle-Katushka Ph-mut construct, the Treacle with 71 deleted serines was amplified by PCR from plasmid pTreacle-GFP Ph-mut with primer set #3 (Supplementary Table 1) using KAPA High-Fidelity DNA Polymerase (KAPA Biosystems, KE2502). The forward and reverse primers contained BglII and BamHI sites respectively. The amplified fragment was inserted into the pKatushka2S-C (Evrogen, FP761) vectors using BglII/BamHI restriction/ligation.

For IPpo-I rDNA damage induction, plasmid pBABe-HA-ER-IppoI (Addgene, #32565) was used.

The pTreacle-GFP S1190/1191 del was constructed based on the pTreacle-GFP plasmid using iProof High-Fidelity DNA polymerase with primer set #11 (Supplementary Table 1). The resulting DNA template after PCR was reprecipitated and treated with the DpnI restriction enzyme. In the next step, the desired DNA template was purified on an agarose gel, phosphorylated with T4 Polynucleotide Kinase (T4 PNK), and ligated.

For the pTOPBP1-FR-BRCTΔ7/8-FK construct, we first amplified TOPBP1-BRCTΔ7/8 from pTOPBP1-FusionRed plasmid using iProof High-Fidelity DNA polymerase with primer set #12 (Supplementary Table 1). The resulting DNA template after PCR was precipitated and treated with the DpnI restriction enzyme. The desired DNA template was purified on an agarose gel, phosphorylated with T4 Polynucleotide Kinase (T4 PNK), and ligated. The FKBP12(F36V) (FK)

fragment was amplified by PCR from the plasmid pLenti PGK FKBP12(F36V)-OGT (Addgene, #154294) with primer set #13 (Supplementary Table 1) digested with BamHI and inserted into pTOPBP1-FR-BRCTΔ7/8 linearized with BamHI.

Construction of the pTOPBP1-FR-ΔAAD-FK was performed as described for the pTOPBP1-FR-BRCTΔ7/8-FK using the primer set #14.

Gene knockdown

RNA interference experiments were performed using Lipofectamine 3000 transfection reagent (Thermo Scientific) following the manufacturer's instructions. The cells were transfected with 50 nM Treacle/TCOF1 (Santa Cruz Biotechnology, #sc-61707) or 50 nM TOPBP1 (Santa Cruz Biotechnology, #sc-41068).

Whole-cell extracts preparation and immunoblotting

Cells were lysed by incubation in RIPA buffer (150 mM NaCl, 1% Triton X-100, 0.5% sodium deoxycholate, 0.1% SDS, 50 mM Tris–HCl (pH 8.0) supplemented with Protease Inhibitor Cocktail (Bimake) and Phosphatase Inhibitor Cocktail (Bimake) for 30 min on ice. Next, the cell extracts were sonicated with a VirSonic 100 ultrasonic cell disrupter and stored at −70°C. The protein concentration was measured by the Bradford assay. Aliquots of each sample were separated by sodium dodecyl sulfate-polyacrylamide gel electrophoresis and blotted onto polyvinylidene difluoride (PVDF) membranes (Amersham/GE Healthcare). The membranes were blocked for 1 h in 2% ECL Advance blocking reagent (GE Healthcare) or 2% bovine serum albumin (BSA) (Sigma-Aldrich) in PBS containing 0.1% Tween 20 (PBS-T) followed by incubation overnight at 4°C with a primary antibody diluted in PBS-T containing 2% blocking reagent or 2% BSA. After three washes with PBS-T, the membranes were incubated for 1 h with the secondary antibodies (horseradish peroxidase-conjugated anti-rabbit or anti-mouse IgG) in PBS-T containing 2% blocking agent or 2% BSA. The immunoblots were visualized using a Pierce ECL plus western blotting substrate. Antibodies used in the study are listed in Supplementary Table 2.

Fluorescence microscopy

For immunostaining, cells were grown on microscope slides. All samples were fixed in CSK buffer (10 mM PIPES, pH 7.0, 100 mM NaCl, 1.5 mM $MgCl_2$, 300 mM sucrose) supplemented with 1% paraformaldehyde (PFA) and 2.5% Triton X-100 for 15 min at room temperature. Cells were washed in PBS and then incubated with antibodies in PBS supplemented with 1% BSA and 0.05% Tween 20 for 1 h at room temperature or overnight at 4°C. Then the cells were washed with PBS three times (5 min each time). The primary antibodies bound to antigens were visualized using

Alexa Fluor 488-conjugated secondary antibodies. The DNA was counterstained with the fluorescent dye 4,6-diamino-2-phenylindole (DAPI) for 10 min at room temperature. The samples were mounted using Dako fluorescent mounting medium (Life Technologies). The immunostained samples were analyzed using a Zeiss AxioScope A.1 fluorescence microscope (objectives: Zeiss N-Achroplan 40 ×/0.65 and EC Plan-Neofluar 100 ×/1.3 oil; camera: Zeiss AxioCam MRm; acquisition software: Zeiss AxioVision Rel. 4.8.2; Jena, Germany) or STELLARIS 5 Leica confocal microscope (objectives: HC PL APO 63x/1.40 oil CS2). The images were processed using ImageJ software (version 1.44) and analyzed using CellProfiler software (version 3.1.5). 3D reconstruction of *xyz* confocal datasets (z-stacks) was performed using Leica LAS-X software. Antibodies used in the study are listed in Supplementary Table 2.

Samples for SIM were mounted in Dako Fluorescence Mounting Medium (Life Technologies) and examined using a Nikon N-SIM microscope (100×/1.49 NA oil immersion objective, 488- and 561-nm diode laser excitation). Image stacks (z-steps of 120 nm) were acquired with an electron-multiplying charge-coupled devices camera (Andor iXon 897; effective pixel size, 60 nm). Exposure conditions were adjusted to get a typical yield of ~5,000 maximum counts (16-bit raw image) while keeping bleaching minimal. Image acquisition, SIM image reconstruction, and data alignment were performed using NIS-Elements (Nikon). 3D reconstruction of x, y, z SIM datasets (z-stacks) was performed using Imaris 7.4 (Bitplane).

Electron microscopy

Twenty-four hours after transfection, cells were fixed with 2.5% neutralized glutaraldehyde in the requisite buffer for 2 h at room temperature, post-fixed with 1% aqueous OsO4, and embedded in Epon. Sections of 100 nm thickness were cut and counterstained with uranyl acetate and lead citrate. Sections were examined and photographed with a JEM 1400 transmission electron microscope (JEOL, Japan) equipped with a QUEMESA bottom-mounted CCD-camera (Olympus SIS, Japan) and operated at 100 kV.

Live-cell imaging

Cells were seeded in 35-mm glass-bottom dishes twelve hours before transfection with the plasmid. Twenty-four hours after transfection, Hoechst 33342 (Cell Signaling Technology) was added to the medium at a final concentration of 1 μg/ml, and the cells were incubated for 20 min at 37°C. Hoechst-containing medium was replaced with a complete fresh medium before the cells underwent live-cell imaging using a STELLARIS 5 Leica confocal microscope equipped with an incubation chamber to provide a humidified atmosphere at 37°C with 5% CO_2. For observation of liquid

droplet behavior, z-stack time-lapses were taken. Maximum intensity projections are shown, but all findings were confirmed on a single plane.

Optodroplet assay

Cells were seeded in 35-mm glass-bottom dishes and were transfected with Treacle-FusionRed-Cry2 plasmid using LTX transfection reagent (Invitrogen) 24 h before imaging. Twenty-four hours after transfection, Hoechst 33342 was added to the medium at a final concentration of 1 μg/ml, and the cells were incubated for 10 min at 37°C. Hoechst-containing medium was replaced with a complete fresh medium before the cells underwent live-cell imaging using a STELLARIS 5 Leica confocal microscope equipped with an incubation chamber to provide a humidified atmosphere at 37°C with 5% CO2. Droplet formation was induced with light pulses at 488 nm (blue light, 1% laser power) for 10 sec, and z-stack images were captured every 60 sec in the absence of blue light.

FRAP analysis

One day prior, imaging cells were transiently transfected with plasmid encoding Treacle-Katushka, TOPBP1-Katushka, or Treacle-FusionRed. FRAP experiments were performed on STELLARIS 5 Leica confocal microscope (objectives: HC PL APO 63x/1.40 oil CS2) equipped with an incubation chamber to provide a humidified atmosphere at 37°C with 5% CO_2. For the bleaching of Treacle-Katushka, TOPBP1-Katushka, or Treacle-FusionRed, a 405-nm laser was used (1% laser power). After bleaching, cells were imaged every 10 sec. Resulted images were analyzed using ImageJ software (version 1.44). The background intensity was subtracted, and values were measured relative to the pre-bleaching time points. For kinetic analysis, relative fluorescence intensity was plotted against time by setting the intensity before bleaching as 100.

Cell sorting

For comet assay or gene transcription analysis one-day prior experiment, cells were transiently transfected with required plasmids using LTX transfection reagent (Invitrogen) or polyethylenimine (PEI). Twenty-four hours after transfection cells were trypsinized and resuspended in PBS and filtered through a nylon membrane to remove cell aggregates. Cell sorting was performed using an SH800 Cell Sorter (Sony) with a laser tuned to 488 nm for GFP fluorescence and 561 nm for FusionRed fluorescence. Gates were set with reference to negative controls. A minimum of 10^5 events was collected for comet assay analysis and 10^6 for gene transcription analysis.

For Chromatin immunoprecipitation (ChIP) analysis twenty-four hours after transfection cells were trypsinized, fixed 1% PFA in 1×PBS for 15 min, then washed three times with 1×PBS

and passed through a 40 mm filter (BD Falcon 352340) to remove cell aggregates. Cell sorting was performed using an SH800 Cell Sorter (Sony) with a laser tuned to 488 nm for GFP fluorescence and 561 nm for FusionRed fluorescence. Gates were set with reference to negative controls. A minimum of $2x10^6$ events was collected for each analysis. The sorted cell fractions were resuspended in a 1x PBS and proceeded to neutral comet assay, ChIP or used to isolate RNA.

Neutral comet assay

After sorting, cell suspension at a concentration of 1×10^5 cells/ml was mixed in a 1:1 ratio with Trevigen LMAgarose (#4250-050-02) at 37°C. The mixture was pipetted onto comet slides (Trevigen) pre-coated with a 1% normal melting point agarose (Sigma-Aldrich) base layer. The drop containing the cells was covered with a glass cover slip and incubated at 4°C for 5 min. After incubation, the coverslips were removed, and the slides were immersed in lysis solution (30 mM EDTA, 0.5% SDS, and 10 mM Tris–HCl, pH 8.0, 500 µg/ml proteinase K) and incubated at 37°C for 1 h. After lysis, the slides were washed three times for 5 min in PBS and incubated in 1×TBE (Tris-Borate-EDTA buffer) for 20 min at 4°C. Electrophoresis was performed in Trevigen electrophoresis system (#4250-050-ES) for 10 min at 4°C and 1 V/cm in 1×TBE. The comets were counterstained with SYBR Green for 1 h (1:3000; Thermo Scientific, #S7563) and then visualized using an inverted Nikon Eclipse Ti-E fluorescence microscope with a Nikon Intensilight C-HGFI light source (objective: Nikon Plan Fluor 4/0.13; camera: DS-Qi2). The images of the comets were analyzed using CellProfiler software (version 2.1.1 rev 6c2d896).

Gene expression analysis

After sorting, cellular RNA was extracted from cells using TRIzol reagent (Life Technologies). All RNA samples were further treated with DNase I (Thermo Scientific) to remove the residual DNA. RNA (1 µg) was reverse transcribed in a total volume of 20 µl for 1 h at 42°C using 0.4 µg of random hexamer primers and 200 U of reverse transcriptase (Thermo Scientific) in the presence of 20 U of ribonuclease inhibitor (Thermo Scientific). The cDNA obtained was analyzed by quantitative polymerase chain reaction (qPCR) using the CFX96 real-time PCR detection system (Bio-Rad Laboratories). The PCRs were performed in 20 µl reaction volumes that included 50 mM Tris–HCl (pH 8.6), 50 mM KCl, 1.5 mM $MgCl_2$, 0.1% Tween-20, 0.5 µM of each primer, 0.2 mM of each dNTP, 0.6 µM EvaGreen (Biotium), 0.2 U of Hot Start Taq Polymerase (Sibenzyme) and 50 ng of cDNA. Primers used in the study are listed in Supplementary Table 3.

Chromatin immunoprecipitation (ChIP)

Cells were fixed for 15 min with 1% formaldehyde at room temperature, and crosslinking was quenched by adding 125 mM glycine for 5 min. Cell sorting was performed if needed. Cells were harvested in PBS, and nuclei were prepared by incubation in FL buffer (5 mM PIPES, pH 8.0, 85 mM KCl, 0.5% NP40) supplemented with Protease Inhibitor Cocktail (Bimake) and Phosphatase Inhibitor Cocktail (Bimake) for 30 min on ice. Next, chromatin was sonicated in RIPA buffer (10 mM Tris–HCl, pH 8.0, 140 mM NaCl, 1% Triton X-100, 0.1% sodium deoxycholate, 0.1% SDS) with a VirSonic 100 to an average length of 200-500 bp. Per ChIP reaction, 10–20 μg chromatin was incubated with 2–4 μg antibodies overnight at 4°C. The next day, Protein A/G Magnetic Beads (Thermo Scientific) were added to each sample and incubated for 4 h at 4°C. Immobilized complexes were washed two times for 10 min at 4°C in low salt buffer (20 mM Tris-HCl, pH 8.0, 150 mM NaCl, 2 mM EDTA, 0.1% SDS, 1% Triton X-100) and high salt buffer (20 mM Tris–HCl, pH 8.0, 500 mM NaCl, 2 mM EDTA, 0.1% SDS, 1% Triton X-100). Samples were incubated with RNase A (Thermo Scientific) for 30 min at room temperature. The DNA was eluted from the beads and de-crosslinked by proteinase K digestion for 4 h at 55°C and subsequent incubation at 65°C for 12 h. Next, DNA was purified using phenol/chloroform extraction and analyzed by qPCR. The qPCR primers used for ChIP analysis are listed in Supplementary Table 4.

rDNA FISH

Cells were fixed with 1% formaldehyde in 1×PBS for 15 min, then washed three times with 1×PBS and permeabilized with 0.5% Triton X-100 for 30 min. After permeabilization, cells were washed three times with 1× PBS. Next, cells were treated with 10 μg/ml RNAse A in 2× SSC at 37°C for at least 45 min, with the following denaturation with 0.1N HCl at room temperature for 15 min. Then cells were washed 2 times with 2× SSC and incubated in 50% formamide in 2× SSC for at least 30 min at room temperature. Fluorescein-labeled probes for human rDNA (BAC clone RP11-450E20) were obtained from Empire Genomics. Cover glasses with cells were denaturized with an rDNA probe in hybridization buffer (2 μl probe and 8 μl of hybridization buffer per cover glass) at 84°C for 7 min and hybridized at 37°C for 24 h. After hybridization, the cells were washed three times (5 min each) with 50% formamide in 2× SSC at 45°C, then twice with 1× SSC at 45°C, and once with 1× SSC at room temperature. Finally, the cells were washed with mQ and stained with DAPI.

Terminal deoxynucleotidyl transferase-mediated labeling and precipitation of DNA lesions (TdT-IP)

Cells were fixed with Streck Tissue Fixative (0.15□M 2-Bromo-2-nitropropane-1,3-diol, 0.1□M Diazolidinyl urea, 0.04□M zinc sulfate heptahydrate, 0.01□M sodium citrate dihydrate and

50 mM EDTA) at room temperature for 20 min. The cells were washed with cold PBS twice and resuspended in Buffer A (0.25% Triton X-100, 10 mM EDTA, 10 mM HEPES, pH 6.5) and Buffer B (200 mM NaCl, 1 mM EDTA, 10 mM HEPES, pH 6.5). After permeabilization of nuclei with Buffer C (100 mM Tris-HCl, pH 7.4, 50 mM EDTA, 1% Triton X-100) for 30 min at 4°C, the nuclei were sequentially washed with cold PBS, deionized water, and 1× TdT reaction buffer (Thermo Scientific). Cells were subsequently incubated in 1 ml reaction buffer (1× TdT buffer (Thermo Scientific), 0.005% Triton X-100, 45 μM biotin-14–dATP (Jena Bioscience), and 250 U TdT (Thermo Scientific) for 90 min at 37°C. Cells were washed twice with ice-cold TBS (50 mM Tris-HCl, pH 7.5, 150 mM NaCl) and then lysed in 200 μl lysis buffer (50 mM Tris-HCl, pH 8.0, 10 mM EDTA, and 1% SDS) for 15 min at 37°C. Chromatin was sheared using the VirSonic 100 to 500 bp of average-size fragments. Diluted and biotinylated DNA fragments were captured with 50 μl of Dynabeads MyOne Streptavidin C1 magnetic beads (Invitrogen) for 4 h at room temperature. Beads were washed three times in 450 μl of RIPA ChIP buffer and twice in 200 μl TE buffer. DNA was analyzed by qPCR. The qPCR primers used for ChIP analysis are listed in Supplementary Table 4.

Proximity ligation assay

After drug treatments or at 24 h post-transfection, cells were fixed for 15 min with 1% formaldehyde at room temperature and permeabilized with 1% Triton X-100. Next, cells were subjected to the proximity ligation assay (PLA) using the Duolink Green, Red or FarRed kit (Sigma-Aldrich) according to the manufacturer's instructions. Briefly, cells were blocked, incubated with appropriate primary antibodies overnight at 4°C, and then incubated with PLA probes, which are secondary antibodies (anti-mouse-IgG and anti-rabbit-IgG) conjugated to unique oligonucleotides. Samples were then treated with a ligation solution followed by an amplification solution containing polymerase and fluorescently labeled oligonucleotides, allowing rolling-circle amplification and detection of discrete fluorescent dots. Some samples after the PLA protocol were additionally counterstained with Alexa-Fluor-488- or Alexa-Fluor-594-conjugated (Molecular Probes) secondary antibody. The DNA was counterstained with DAPI for 10 min at room temperature. The samples were mounted using Dako fluorescent mounting medium (Life Technologies) and analyzed using STELLARIS 5 Leica confocal microscope (objectives: HC PL APO 63x/1.40 oil CS2). The images were analyzed using ImageJ software (version 1.44).

Phosphopeptide enrichment for LC-MS/MS analysis

To enrich samples for phosphorylated peptides, we applied the High-Select TiO2 Phosphopeptide Enrichment Kit (Thermo Fisher) according to the manufacturer's protocol. Briefly, HeLa cells were

transfected with Treacle-Katushka, and twenty-four hours after transfection, 10^7 cells were washed three times with PBS, lysed in buffer containing 4% SDS, 100 mM Tris-HCl (pH 8.0) with phosphatase inhibitor cocktails 1 and 2 (Sigma-Aldrich), and incubated at 60°C for 30 min. The cell lysates were subjected to sonication on ice (3 cycles: 10 sec on/off pulses with a 30% amplitude). Disulfide bonds were reduced with DTT (5 mM) for 30 min at room temperature (RT). Afterward, iodoacetamide was added to a final concentration of 10 mM. The samples were incubated at RT for 20 min in the dark, and the reaction was stopped by adding 5 mM DTT. After the precipitation of proteins using methanol/chloroform, the semi-dry protein pellet was dissolved in 50 µL of 8 M urea, 2 M thiourea, and 10 mM Tris-HCl (pH 8.0). Then, protein amounts were adjusted to 0.5 mg using the Quick Start Bradford protein assay (Bio-Rad), and samples were diluted with ammonium bicarbonate solution to reduce urea concentration to 2 M. Trypsin (Promega) was added at the ratio of 1:100 w/w, and the samples were incubated for 14 h at 37°C. The reaction was stopped by adding formic acid to the final concentration of 5%. The tryptic peptides were desalted using SDB-RPS membrane (SigmaAldrich) and vacuum-dried. Then, the phosphoenrichment procedure was performed according to the manufacturer's protocol. Before LC-MS/MS analysis, samples were redissolved in 5% acetonitrile with 0.1% trifluoroacetate solution and sonicated.

LC-MS/MS Analysis

Proteomic analysis was performed using a Q Exactive HF mass spectrometer. Samples were loaded onto 50-cm columns packed in-house with C18 3 µM Acclaim PepMap 100 (Thermo Fisher), with an Ultimate 3000 Nano LC System (Thermo Fisher) coupled to the MS (Q Exactive HF, Thermo Fisher). Peptides were loaded onto the column thermostatically controlled at 40°C in buffer A (0.2% Formic acid) and eluted with a linear (120 min) gradient of 4 to 55% buffer B (0.1% formic acid, 80% acetonitrile) in buffer A at a flow rate of 350 nl/min. Mass spectrometric data were stored during automatic switching between MS1 scans and up to 15 MS/MS scans (topN method). The target value for MS1 scanning was set to 3×10^6 in the range 300–1200 m/z with a maximum ion injection time of 60 ms and a resolution of 60000. The precursor ions were isolated at a window width of 1.4 m/z and a fixed first mass of 100.0 m/z. Precursor ions were fragmented by high-energy dissociation in a C-trap with a normalized collision energy of 28 eV. MS/MS scans were saved with a resolution of 15000 at 400 m/z and at a value of 1×10^5 for target ions in the range of 200–2000 m/z with a maximum ion injection time of 30 ms.

Protein identification and spectral counting

Raw LC-MS/MS data from Q Exactive HF mass spectrometer were converted to .mgf peak lists with MSConvert (ProteoWizard Software Foundation). For this procedure, we used the following

parameters: "--mgf --filter peakPicking true". For protein identification, the generated peak lists were searched with MASCOT (version 2.5.1, Matrix Science Ltd., UK) and X! Tandem (ALANINE, 2017.02.01, 2017.02.01, The Global Proteome Machine Organization) search engines against UniProt human protein knowledgebase with the concatenated reverse decoy dataset. The precursor and fragment mass tolerance were set at 20 ppm and 0.04 Da, respectively. Database-searching parameters included the following: tryptic digestion with one possible missed cleavage, static modification for carbamidomethyl (C), and dynamic/flexible modifications for oxidation (M) and phosphorylation (S, T, Y). For X! Tandem, we also selected parameters that allowed a quick check for protein N-terminal residue acetylation, peptide N-terminal glutamine ammonia loss, or peptide N-terminal glutamic acid water loss. Result files were submitted to Scaffold 5 software (version 5.1.0) for validation and meta-analysis. We used the local false discovery rate scoring algorithm with standard experiment-wide protein grouping. For the evaluation of peptide and protein hits, a false discovery rate of 5% was selected for both. False positive identifications were based on reverse database analysis. We also set protein annotation preferences in Scaffold to highlight Swiss-Prot accessions among others in protein groups. Additionally, raw LC-MS/MS data from Q Exactive HF mass spectrometer were analyzed with MaxQuant (version 1.6.10.43) against UniProt human protein knowledgebase. For this procedure, we used the following parameters: Orbitrap instrument type, tryptic digestion with one possible missed cleavage, fixed modification for carbamidomethyl (C), variable modifications for oxidation (M), acetyl (protein N-term) and phosphorylation (S, T, Y), LFQ label-free quantification.

Acknowledgments

This work was supported by RSF grant 21-74-10018. Confocal microscopy studies were supported by grant 075-15-2019-1661 from the Ministry of Science and Higher Education of the Russian Federation. LC-MS/MS analyses were performed using the equipment of the Center for Precision Genome Editing and Genetic Technologies for Biomedicine, Lopukhin Federal Research and Clinical Center of Physical-Chemical Medicine of Federal Medical Biological Agency.

Author contributions: O.L.K., A.K.V., and S.V.R. conceived the study. A.K.V. and O.L.K. designed the experiments. A.K.V., A.P.K., A.V.L., and D.A.D. performed most of the experiments. V.O.S. and G.P.A. performed and analyzed mass-spectrometry experiments. E.P.K. and I.I.K. performed transmission electron microscopy imaging. O.L.K. and A.K.V. wrote the manuscript with assistance from the other authors.

Competing interests: The authors declare no competing interests.

Data and materials availability: All data needed to evaluate the conclusions in the paper are present in the paper and/or the Supplementary Materials.

References

Banani SF, Lee HO, Hyman AA, Rosen MK (2017) Biomolecular condensates: organizers of cellular biochemistry. ***Nat Rev Mol Cell Biol*** **18**: 285-298

Bax BD, Murshudov G, Maxwell A, Germe T (2019) DNA Topoisomerase Inhibitors: Trapping a DNA-Cleaving Machine in Motion. ***J Mol Biol*** **431**: 3427-3449

Cerqueira AV, Lemos B (2019) Ribosomal DNA and the Nucleolus as Keystones of Nuclear Architecture, Organization, and Function. ***Trends Genet*** **35**: 710-723

Ciccia A, Huang JW, Izhar L, Sowa ME, Harper JW, Elledge SJ (2014) Treacher Collins syndrome TCOF1 protein cooperates with NBS1 in the DNA damage response. ***Proc Natl Acad Sci U S A*** **111**: 18631-18636

Day M, Oliver AW, Pearl LH (2021) Phosphorylation-dependent assembly of DNA damage response systems and the central roles of TOPBP1. ***DNA Repair (Amst)*** **108**: 103232

Falahati H, Pelham-Webb B, Blythe S, Wieschaus E (2016) Nucleation by rRNA Dictates the Precision of Nucleolus Assembly. ***Curr Biol*** **26**: 277-285

Falahati H, Wieschaus E (2017) Independent active and thermodynamic processes govern the nucleolus assembly in vivo. ***Proc Natl Acad Sci U S A*** **114**: 1335-1340

Feric M, Vaidya N, Harmon TS, Mitrea DM, Zhu L, Richardson TM, Kriwacki RW, Pappu RV, Brangwynne CP (2016) Coexisting Liquid Phases Underlie Nucleolar Subcompartments. ***Cell*** **165**: 1686-1697

Franzmann TM, Alberti S (2019) Protein Phase Separation as a Stress Survival Strategy. ***Cold Spring Harb Perspect Biol*** **11**

Frattini C, Promonet A, Alghoul E, Vidal-Eychenie S, Lamarque M, Blanchard MP, Urbach S, Basbous J, Constantinou A (2021) TopBP1 assembles nuclear condensates to switch on ATR signaling. ***Mol Cell*** **81**: 1231-1245 e1238

Gal Z, Nieto B, Boukoura S, Rasmussen AV, Larsen DH (2022) Treacle Sticks the Nucleolar Responses to DNA Damage Together. ***Front Cell Dev Biol*** **10**: 892006

Gonzales B, Henning D, So RB, Dixon J, Dixon MJ, Valdez BC (2005) The Treacher Collins syndrome (TCOF1) gene product is involved in pre-rRNA methylation. ***Hum Mol Genet*** **14**: 2035-2043

Grzanka M, Piekielko-Witkowska A (2021) The Role of TCOF1 Gene in Health and Disease: Beyond Treacher Collins Syndrome. ***Int J Mol Sci*** **22**

Harding SM, Boiarsky JA, Greenberg RA (2015) ATM Dependent Silencing Links Nucleolar Chromatin Reorganization to DNA Damage Recognition. ***Cell Rep*** **13**: 251-259

Ide S, Imai R, Ochi H, Maeshima K (2020) Transcriptional suppression of ribosomal DNA with phase separation. ***Sci Adv*** **6**

Isaac C, Marsh KL, Paznekas WA, Dixon J, Dixon MJ, Jabs EW, Meier UT (2000) Characterization of the nucleolar gene product, treacle, in Treacher Collins syndrome. ***Mol Biol Cell*** **11**: 3061-3071

Korsholm LM, Gal Z, Lin L, Quevedo O, Ahmad DA, Dulina E, Luo Y, Bartek J, Larsen DH (2019) Double-strand breaks in ribosomal RNA genes activate a distinct signaling and chromatin response to facilitate nucleolar restructuring and repair. ***Nucleic Acids Res*** **47**: 8019-8035

Lafontaine DLJ, Riback JA, Bascetin R, Brangwynne CP (2021) The nucleolus as a multiphase liquid condensate. ***Nat Rev Mol Cell Biol*** **22**: 165-182

Larsen DH, Hari F, Clapperton JA, Gwerder M, Gutsche K, Altmeyer M, Jungmichel S, Toledo LI, Fink D, Rask MB *et al* (2014) The NBS1-Treacle complex controls ribosomal RNA transcription in response to DNA damage. ***Nat Cell Biol* 16**: 792-803

Lin CI, Yeh NH (2009) Treacle recruits RNA polymerase I complex to the nucleolus that is independent of UBF. ***Biochem Biophys Res Commun* 386**: 396-401

Mehta S, Zhang J (2022) Liquid-liquid phase separation drives cellular function and dysfunction in cancer. ***Nat Rev Cancer* 22**: 239-252

Mittag T, Pappu RV (2022) A conceptual framework for understanding phase separation and addressing open questions and challenges. ***Mol Cell* 82**: 2201-2214

Mooser C, Symeonidou IE, Leimbacher PA, Ribeiro A, Shorrocks AK, Jungmichel S, Larsen SC, Knechtle K, Jasrotia A, Zurbriggen D *et al* (2020) Treacle controls the nucleolar response to rDNA breaks via TOPBP1 recruitment and ATR activation. ***Nat Commun* 11**: 123

Park A, Won ST, Pentecost M, Bartkowski W, Lee B (2014) CRISPR/Cas9 allows efficient and complete knock-in of a destabilization domain-tagged essential protein in a human cell line, allowing rapid knockdown of protein function. ***PLoS One* 9**: e95101

Regulus P, Duroux B, Bayle PA, Favier A, Cadet J, Ravanat JL (2007) Oxidation of the sugar moiety of DNA by ionizing radiation or bleomycin could induce the formation of a cluster DNA lesion. ***Proc Natl Acad Sci U S A* 104**: 14032-14037

Reynolds RC, Montgomery PO, Hughes B (1964) Nucleolar "Caps" Produced by Actinomycin D. ***Cancer Res* 24**: 1269-1277

Sabari BR, Dall'Agnese A, Young RA (2020) Biomolecular Condensates in the Nucleus. ***Trends Biochem Sci* 45**: 961-977

Shcherbo D, Merzlyak EM, Chepurnykh TV, Fradkov AF, Ermakova GV, Solovieva EA, Lukyanov KA, Bogdanova EA, Zaraisky AG, Lukyanov S *et al* (2007) Bright far-red fluorescent protein for whole-body imaging. ***Nat Methods* 4**: 741-746

Shin Y, Berry J, Pannucci N, Haataja MP, Toettcher JE, Brangwynne CP (2017) Spatiotemporal Control of Intracellular Phase Transitions Using Light-Activated optoDroplets. ***Cell* 168**: 159-171 e114

Talukdar A, Kundu B, Sarkar D, Goon S, Mondal MA (2022) Topoisomerase I inhibitors: Challenges, progress and the road ahead. ***Eur J Med Chem* 236**: 114304

Valdez BC, Henning D, So RB, Dixon J, Dixon MJ (2004) The Treacher Collins syndrome (TCOF1) gene product is involved in ribosomal DNA gene transcription by interacting with upstream binding factor. ***Proc Natl Acad Sci U S A* 101**: 10709-10714

Velichko AK, Ovsyannikova N, Petrova NV, Luzhin AV, Vorobjeva M, Gavrikov AS, Mishin AS, Kireev, II, Razin SV, Kantidze OL (2021) Treacle and TOPBP1 control replication stress response in the nucleolus. ***J Cell Biol* 220**

Velichko AK, Petrova NV, Luzhin AV, Strelkova OS, Ovsyannikova N, Kireev, II, Petrova NV, Razin SV, Kantidze OL (2019) Hypoosmotic stress induces R loop formation in nucleoli and ATR/ATM-dependent silencing of nucleolar transcription. ***Nucleic Acids Res* 47**: 6811-6825

Woodruff JB, Ferreira Gomes B, Widlund PO, Mahamid J, Honigmann A, Hyman AA (2017) The Centrosome Is a Selective Condensate that Nucleates Microtubules by Concentrating Tubulin. ***Cell* 169**: 1066-1077 e1010

Figure Legends

Fig. 1. Treacle drives the formation of nuclear condensates. (A) HeLa cells were transfected with opto-Treacle (Treacle-FusionRed-Cry2) construct. Formation of opto-Treacle drops was induced with blue light illumination of the cells for 10 sec. Representative images are shown. (B) HeLa cells were transfected with Treacle-Katushka at low (50 ng plasmids per $2x10^5$ cells) and high concentration (1000 ng plasmids per $2x10^5$ cells) and, 24 h after transfection, fixed and DAPI-stained (gray). (C) HeLa cells were processed as described in (B) and analyzed by laser scanning confocal microscopy. Surface reconstructions of Treacle-Katushka drops are shown in the right panel. Graphs illustrate quantification in arbitrary units of the 3D analysis of Treacle-Katushka drops' shape by IMARIS software. Sphere form factor = sphere area/particle area. (D) Transiently transfected with Treacle-Katushka HeLa cells were treated with 0,05µg/ml actinomycin D to induce rDNA transcriptional repression and imaged for 120 minutes. (E) Time-lapse imaging of HeLa cells transiently transfected with Treacle-Katushka at high concentration. Representative images of Treacle-Katushka drop fusion events are shown (magnified images). Graphs illustrate the frequency of fusion Treacle-droplets per cell for 12 hours. The calculation is presented for 6 biological replicates of 10 cells each. (F) Kinetics of nucleolar Treacle-Katushka was studied by FRAP. One fibrillar center or nucleolar cap that was induced by actinomycin D was bleached, and fluorescence recovery was monitored. The shaded parts of the lines represent SD, n = 5. (G) HeLa cells were transiently transfected with Treacle-Katushka. FRAP analysis of Treacle-Katushka drop dynamics was performed. Representative time-lapse images of photobleached Treacle-Katushka drop are shown. Graphs illustrate the quantification of the Treacle- Katushka FRAP analysis described in (F).

Fig. 2. Structural grounds of Treacle's phase separation. (A) Schematic showing the layout of conserved domains and motifs in Treacle as well as Katushka- or GFP-tagged deletion mutants of Treacle, lacking either N-terminal region (D1), both N-terminal and central repeat regions (D1,2), C-terminal region (D3), both central repeat and C-terminal regions (D2,3) or both N-terminal region and C-terminal regions (D1,3). (B) HeLa cells were transiently transfected with plasmid constructs encoding Katushka-fused full-length Treacle or Katushka-fused Treacle deletion mutants at high concentration (1000 ng plasmids per $2x10^5$ cells) and, 24 h after transfection, fixed and DAPI-stained (gray). (C) HeLa cells were processed as described in (B). The number of Treacle-Katushka drops per cell was measured (n>40). (D) The structure of the most common isoform of Treacle (Treacle isoform d, 1488 amino acids, NP_001128715.1). The scheme shows the positions of CK2- and PIKK-dependent phospho-serines found in the phospho-proteomic analysis. (E) HeLa cells were transiently transfected with plasmid constructs encoding Katushka-fused wild-type Treacle (wt) or Katushka-fused Treacle with deleted 71 serines in CK2 consensus sites (Treacle-Katushka Ph-mut) at high concentration (1000 ng plasmids per $2x10^5$ cells) and, 24 h after transfection, were

fixed and DAPI-stained (gray). The number of Treacle-Katushka wild type (wt) and Treacle-Katushka Ph-mut drops per cell (n>40) were measured. (F) HeLa cells were transiently transfected with plasmid constructs encoding Katushka-fused full-length wild-type Treacle, Katushka-fused Treacle lacking both N-terminal and central repeat region (D1,2 mutant), or Katushka-fused Ph-mutant at low concentration (50 ng plasmids per $2x10^5$ cells). 24 h after transfection, cells were fixed, DAPI-stained (gray), and analyzed by 3D-SIM microscopy.

Fig. 3. Phase separation of Treacle is necessary for ribosomal transcription. (A) Intact or transiently transfected with Treacle-Katushka HeLa cells were immunostained for Treacle (magenta) and RPA194 or UBF (green) and analyzed by LSCM. The DNA was stained with DAPI (gray). (B) Endogenous Treacle-depleted cells were transfected with plasmid constructs encoding GFP-fused full-length wild-type Treacle (wt), GFP-fused Treacle lacking N-terminal region (D1), GFP-fused Treacle lacking both N-terminal and central repeat region (D1,2 mutant), or GFP-fused Ph-mutant. 24 h after transfection, GFP-positive cells were collected using FACS and used for chromatin immunoprecipitation with GFP, UBF1 or RPA194 antibodies or for RNA extraction. ChIP was followed by qPCR using the A1 primers to the promoter of rRNA gene. Data are represented relative to the input. Values are means ±SD from at least three independent replicates.

Fig. 4. Treacle forms cooperative biomolecular condensates with TOPBP1. (A) HeLa cells transiently transfected with opto-Treacle were blue light illuminated for 10 sec to induce opto-Treacle drop formation, fixed 5 min later, and immunostained with antibodies against TOPBP1 (green). DNA was stained with DAPI (gray). Colocalization analysis of opto-Treacle and TOPBP1 was performed. Graphs show quantification in arbitrary units of the distribution of TOPBP1 and opto-Treacle fluorescence along the lines shown in the figure. (B) HeLa cells were transfected with Treacle-Katushka, fixed, and immunostained with anti-TOPBP1 antibodies (green). (C) HeLa cells transiently transfected with Treacle-Katushka (magenta) were subjected to proximity ligation assay (PLA) with antibodies against TOPBP1 and Treacle. DNA was stained with DAPI (gray). PLA detection of Treacle-TOPBP1 interactions is visible as distinct green fluorescent dots in Treacle-Katushka drops. (D) HeLa cells were transfected with Treacle-Katushka S1190/1191 del mutant, fixed, and immunostained with anti-TOPBP1 antibodies (green). (E) HeLa cells were transfected with Treacle-Katushka wild type (wt) or S1190/1191 del mutant, fixed, and immunostained with anti-TOPBP1 antibodies. The proportion of TOPBP1-positive Treacle-Katushka drops is shown. (F) HeLa cells were processed as described in (E) and subjected to proximity ligation assay (PLA) with antibodies against TOPBP1 and Treacle. Graphs illustrate the quantification of PLA signal intensity per Treacle-Katushka drop. (G) HeLa cells were transiently transfected with Treacle-Katushka (magenta) and treated with either PIKK inhibitor wortmannin (50 μM; 6 h), or CK2 kinase inhibitor CX-4945 (30 μM; 6 h). The cells were then fixed and immunostained with anti-TOPBP1 antibodies

(green). (H) HeLa cells were processed as described in (G). The proportion of TOPBP1-positive Treacle-Katushka drops is shown. (I) HeLa cells were processed as described in (G) and subjected to PLA with antibodies against TOPBP1 and Treacle. Graphs illustrate the quantification of PLA signal intensity per Treacle-Katushka drop. (J) HeLa cells were transiently transfected with plasmid constructs encoding Katushka-fused full-length wild-type Treacle (wt), Katushka-fused Treacle lacking N-terminal region (D1), Katushka-fused Treacle lacking both N-terminal and central repeat region (D1,2 mutant), or Katushka-fused Ph-mutant. The cells were then fixed and immunostained with an anti-TOPBP1 antibody (green). The DNA was stained with DAPI (gray). (K) HeLa cells were processed as described in (J) and subjected to PLA with antibodies against TOPBP1 and Treacle. Graphs illustrate the quantification of PLA signal intensity per Treacle-Katushka drop.

Fig. 5. Cooperative Treacle-TOPBP1 biomolecular condensates promote DDR. (A) HeLa cells were transiently transfected with Treacle-GFP or co-transfected with Treacle-GFP and TOPBP1-FusionRed at different ratios (the quantity of plasmid DNA (ng) per $2x10^5$ cells is indicated on the figure panels). 24 h after transfection, cells were fixed and immunostained with anti-γH2AX antibodies (red). The DNA was stained with DAPI (gray). (B) HeLa cells were processed as described in (A). The proportion of γH2AX-positive Treacle-TOPBP1 drops is shown. (C) HeLa cells were transiently transfected with Treacle-Katushka for TT droplet formation or with TOPBP1-FusionRed for mTT droplet formation. 24 h after transfection, the cells were fixed and subjected to proximity ligation assay (PLA) with antibodies against TOPBP1 and Treacle. DNA was stained with DAPI (gray). Graphs illustrate the quantification of PLA signal intensity per Treacle-Katushka drop. (D) HeLa cells were processed as described in (A). 24 h after transfection, cells were subjected to cell sorting into GFP-positive or GFP/FusionRed (FR)-positive populations, and collected fractions were used for ChIP with γH2AX antibodies. ChIP was followed by qPCR using the rDNA amplicons positioned as indicated on the scheme. Sequences from the GAPDH gene and Alu repeats were used as controls. Data are represented relative to the input. Values are means ±SD from at least three independent replicates. (E) HeLa cells were processed as described in (A). 24 h after transfection, cells were subjected to cell sorting into GFP-positive or GFP/FR-positive populations. The sorted cell fractions were used for RNA extraction. RT-qPCR was performed; it shows levels of pre-rRNA normalized to GAPDH mRNA. Values are mean ± SD. (F) HeLa cells transiently co-transfected with Treacle-GFP and TOPBP1-FusionRed for mTT droplet formation (merge mangenta+green). 24 h after transfection, the cells were fixed and immunostained for either 53BP1, BRCA1, MDC1, Nbs1, phospho-ATM (pATM; Ser1981) or phospho-ATR (pATR; Ser1989) (red). DNA was stained with DAPI (gray). The images were analyzed by laser scanning confocal microscopy. (G) DNA damage in rDNA was studied in HeLa cells transfected with Treacle-GFP for TT drop formation or co-transfected with Treacle-GFP and TOPBP1-FusionRed for mTT drop formation. For rDNA damage induction, HeLa cells were transfected with I-PpoI and

treated with 4-hydroxytamoxifen to activate it. TdT-IP was followed by qPCR using the rDNA amplicons positioned as indicated on the scheme below the graphs. Data are represented relative to the input. Values are mean ± SD from at least three independent experiments.

Fig. 6. ATR-dependent oligomerization of TOPBP1 within Treacle condensates is necessary for DDR activation. (A) Treacle-depleted cells were transfected with plasmid constructs encoding TOPBP1-FusionRed (FR), fixed and immunostained with anti-γH2AX antibodies (red). The DNA was stained with DAPI (gray). (B) HeLa cells were processed as described in (A). 24 h after transfection, FR-positive cells were collected by FACS and used for RNA extraction. qRT-PCR was performed. RT-qPCR shows levels of pre-rRNA normalized to GAPDH mRNA. Values are mean ± SD. (C) HeLa cells were processed as described in (A). 24 h after transfection, FR-positive cells were collected by FACS and used for ChIP analysis with anti-γH2AX antibodies. ChIP was followed by qPCR using the rDNA amplicons positioned as indicated on the scheme in Fig. 5D. GAPDH and Alu were used as controls. Data are represented relative to the input. Values are means ±SD from at least three independent replicates. (D) HeLa cells transiently co-transfected with Treacle-GFP and TOPBP1-FusionRed for mTT drop formation. 24 h after transfection, the cells were treated with 15 µM VE-821 for 6 h, fixed and immunostained with anti-γH2AX antibodies (red). The DNA was stained with DAPI (gray). (E) HeLa cells were processed as described in (D). 24 h after transfection, GFP/FR-positive cells were collected by FACS and used for RNA extraction. qRT-PCR was performed. RT-qPCR shows levels of pre-rRNA normalized to GAPDH mRNA. Values are mean ± SD. (F) HeLa cells were processed as described in (D). 24 h after transfection, GFP/FR-positive cells were collected by FACS and used for ChIP analysis with anti-γH2AX antibodies. ChIP was followed by qPCR using the rDNA amplicons positioned as indicated on the scheme in Fig. 5D. GAPDH and Alu were used as controls. Data are represented relative to the input. Values are means ±SD from at least three independent replicates. (G) HeLa cells transiently transfected with Treacle-GFP or co-transfected with Treacle-GFP and TOPBP1-FusionRed at the different ratios. 24 h after transfection, cells were subjected to cell sorting into GFP-positive or GFP/FR-positive populations. The sorted cell fractions were used for ChIP with phospho-ATR (pATR; Ser1989) antibodies. ChIP was followed by qPCR using the rDNA amplicons positioned as indicated on the scheme in Fig. 5D. GAPDH and Alu were used as control. Data are represented relative to the input. Values are means ±SD from at least three independent replicates. (H) HeLa cells were transiently transfected with Treacle-GFP or Treacle-GFP S1190/1191 del mutant for TT drop formation or co-transfected with a combination of Treacle-GFP and TOPBP1-FusionRed, or Treacle-GFP S1190/1191 del mutant and TOPBP1-FusionRed for mTT drop formation. 24 h after transfection, the cells were treated with 15 µM VE-821 or 30 µM CX-4945 for 6 h, fixed and subjected to proximity ligation assay (PLA) with antibodies against TOPBP1 and GFP. Graphs illustrate the quantification of PLA signal intensity per Treacle-GFP

drop. (I) HeLa cells were transiently co-transfected with a combination of Treacle-GFP and TOPBP1-FR-ΔBRCT7/8-FK or Treacle-GFP and TOPBP1-FR-ΔAAD-FK and if necessary treated with 100 nM AP20187 for 24 hours. 24 h after transfection, were fixed and immunostained with anti-γH2AX antibodies (red). The DNA was stained with DAPI (gray). (J) HeLa cells were processed as described in (I). 24 h after transfection, cells were subjected to cell sorting into GFP/FR-positive populations. The sorted cell fractions have proceeded to chromatin immunoprecipitation with γH2AX antibodies. ChIP was followed by qPCR using the rDNA amplicons positioned as indicated on the scheme in Fig. 5D. GAPDH and Alu were used as control. Data are represented relative to the input. Values are means ±SD from at least three independent replicates. (K) HeLa cells were processed as described in (I). 24 h after transfection, cells were subjected to cell sorting into GFP/FR-positive populations. After sorting cells were used for RNA extraction. qRT-PCR was performed. RT-qPCR shows levels of pre-rRNA normalized to GAPDH mRNA. Values are mean ± SD. (L) HeLa cells were transiently co-transfected with a combination of Treacle-GFP and TOPBP1-FR-ΔBRCT7/8-FK or Treacle-GFP and TOPBP1-FR-ΔAAD-FK and if necessary treated with 100 nM AP20187 for 24 hours. 24 h after transfection, were fixed and subjected to PLA with antibodies against TOPBP1 and GFP. Graphs illustrate the quantification of PLA signal intensity per Treacle-GFP drop.

Fig. 7. Treacle-TOPBP1 condensate formation is essential for ribosomal DDR and DNA repair. (A) DNA damage induction in rDNA was studied in control (DMSO-treated) HeLa cells, HeLa cells treated with CPT (1 μM, 30 min), VP16 (90 μM, 30 min), or Bleo (100 μM, 30 min). Cells were immunostained for TOPBP1 (green) and Ki67 (gray). One representative image is shown in each case. (B) Quantification of the cells described in (A). The proportion of cells containing nucleolar TOPBP1 foci is shown. (C) VP16-treated (90 μM, 30 min) HeLa cells were stained for Treacle (magenta) and TOPBP1 (green) and analyzed by LSCM. The DNA was stained with DAPI (gray). Co-localization analysis was performed on the merged images. Graphs illustrate quantification in arbitrary units of Treacle and TOPBP1 fluorescence distribution along the lines shown in the figures. (D) ChIP-seq distributions of Treacle and TOPBP1 on a ribosomal unit of chromosome 21 from control cells (DMSO-treated) and cells treated with VP16 (90 μM, 30 min). (E) Control (DMSO-treated) HeLa cells and HeLa cells treated with VP16 (90 μM, 30 min) were subjected to PLA with antibodies against TOPBP1 and Treacle. DNA was stained with DAPI (gray). PLA detection of Treacle-TOPBP1 interactions is visible as distinct green, fluorescent dots. (F) HeLa cells were treated with either VP16 (90 μM), preincubated with 15 μM VE-821 or 30 μM CX-4945 for 6 h and then treated with VP16 (90 μM), or treated with VP16 (90 μM) and next incubated with 10% 1,6-HD for 5 min or 500 mM NaCl for 30 min. ChIP experiments were performed with antibodies against TOPBP1. ChIP was followed with qPCR using the rDNA amplicons positioned as indicated on the scheme. Data are represented relative to the input. Values

are means ±SD from at least three independent replicates. (G) Occupancy of TOPBP1 at the rDNA of VP16-treated control and Treacle knockdown (kd) HeLa cells. ChIP was performed as described in (F). (H) Treacle-depleted cells were transfected with plasmid constructs encoding GFP-fused full-length wild-type Treacle (wt), GFP-fused Treacle lacking the N-terminal region (D1), GFP-fused Treacle lacking both N-terminal and central repeat region (D1,2 mutant), GFP-fused Treacle S1190/1191 del mutant or GFP-fused Ph-mutant. 24 h after transfection, cells were treated with 90 μM VP16, fixed and subjected to cell sorting into GFP-positive populations. The sorted cell fractions were used for ChIP with TOPBP1 antibodies. ChIP was followed by qPCR using the A1 primers to the promoter of the rRNA gene. Data are represented relative to the input. Values are means ±SD from at least three independent replicates. (I) Transiently transfected with Treacle-Katushka at low concentration, HeLa cells were treated with 90 μM VP16 to induce DNA breaks and imaged for 60 minutes. Representative examples of Treacle-Katushka fusions (magnified regions) are shown. (J) Intact (mock-treated) HeLa cells and HeLa cells depleted for either TOPBP1 or Treacle were treated with DMSO (mock), or VP16 (90 μM, 30 min). qRT-PCR was performed. Levels of pre-rRNA normalized to GAPDH mRNA are shown. Values are mean ± SD. (K) HeLa cells depleted for Treacle were transfected with plasmid constructs encoding GFP-fused full-length wild-type Treacle (wt), GFP-fused Treacle lacking both N-terminal and central repeat region (D1,2 mutant), or GFP-fused Ph-mutant. Intact cells were used as a control. 24 h after transfection, cells were treated with 90 μM VP16, fixed and subjected to cell sorting into GFP-positive populations. The sorted cell fractions have proceeded to ChIP with phospho-ATR (pATR; Ser1989) or γH2AX antibodies. ChIP was followed by qPCR using the A1 primers to the promoter of the rRNA gene. Data are represented relative to the input. Values are means ±SD from at least three independent replicates. (L) Control HeLa (mock) cells and HeLa cells depleted for Treacle or TOPBP1 were treated with VP16 for 30 min and then incubated in a fresh culture medium for 0, 6, 12, or 24 h. rDNA locus-specific DNA damage was assessed by the TdT-IP followed by qPCR with an rDNA promoter amplicon (A1). Data are represented relative to the input. Values are means ±SD from at least three independent replicates.

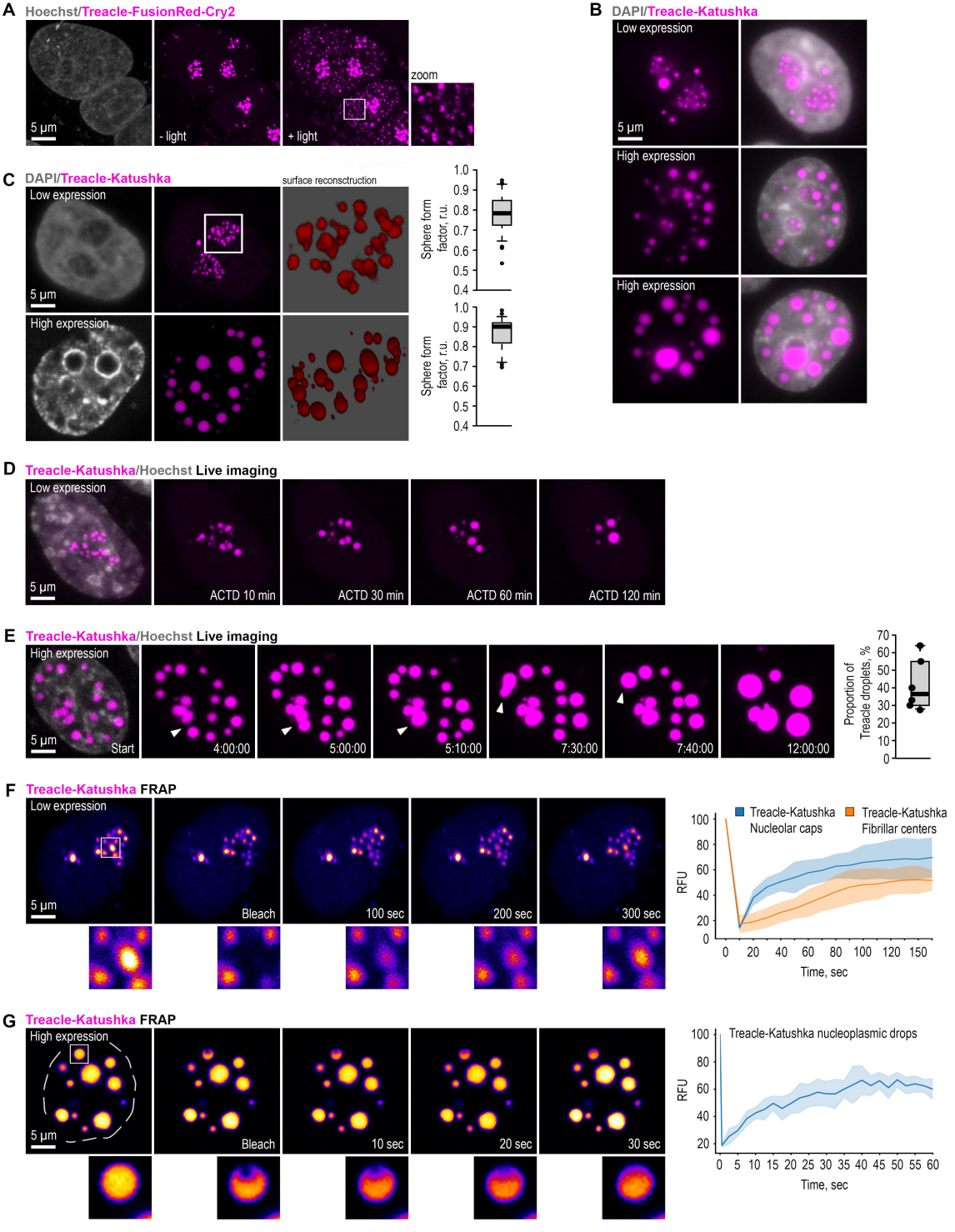
A
Hoechst/Treacle-FusionRed-Cry2
5 µm
- light
+ light
zoom
B
DAPI/Treacle-Katushka
Low expression
5 µm
High expression
High expression
C
DAPI/Treacle-Katushka
surface reconsctruction
Low expression
5 µm
High expression
Sphere form factor, r.u.
1.0
0.9
0.8
0.7
0.6
0.5
0.4
D
Treacle-Katushka/Hoechst Live imaging
Low expression
5 µm
ACTD 10 min
ACTD 30 min
ACTD 60 min
ACTD 120 min
E
Treacle-Katushka/Hoechst Live imaging
High expression
5 µm
Start
4:00:00
5:00:00
5:10:00
7:30:00
7:40:00
12:00:00
Proportion of Treacle droplets, %
70
60
50
40
30
20
10
0
F
Treacle-Katushka FRAP
Low expression
5 µm
Bleach
100 sec
200 sec
300 sec
Treacle-Katushka Nucleolar caps
Treacle-Katushka Fibrillar centers
RFU
100
80
60
40
20
0
0
20
40
60
80
100
120
150
Time, sec
G
Treacle-Katushka FRAP
High expression
5 µm
Bleach
10 sec
20 sec
30 sec
Treacle-Katushka nucleoplasmic drops
RFU
100
80
60
40
20
0
5
10
15
20
25
30
35
40
45
50
55
60
Time, sec

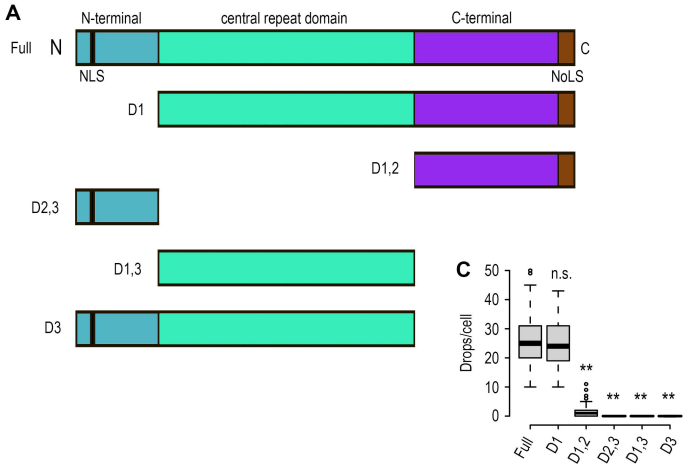
A
N-terminal
central repeat domain
C-terminal
Full
N
C
NLS
NoLS
D1
D1,2
D2,3
D1,3
D3
C
Drops/cell
n.s.
**
Full
D1
D1,2
D2,3
D1,3
D3

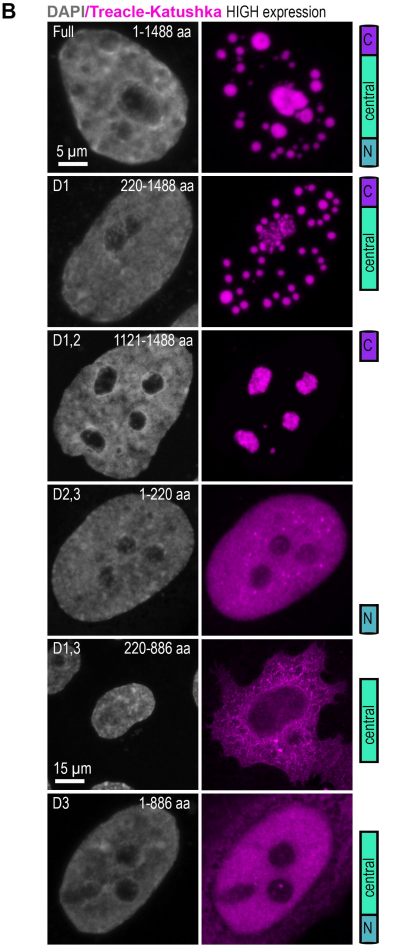
B
DAPI/Treacle-Katushka HIGH expression
Full 1-1488 aa
5 µm
D1 220-1488 aa
D1,2 1121-1488 aa
D2,3 1-220 aa
D1,3 220-886 aa
15 µm
D3 1-886 aa
C
central
N

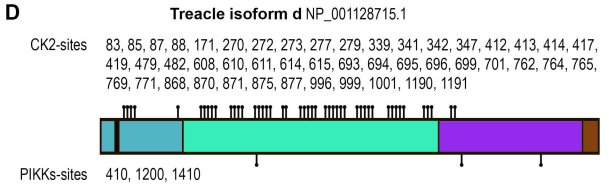
D
Treacle isoform d NP_001128715.1
CK2-sites
83, 85, 87, 88, 171, 270, 272, 273, 277, 279, 339, 341, 342, 347, 412, 413, 414, 417, 419, 479, 482, 608, 610, 611, 614, 615, 693, 694, 695, 696, 699, 701, 762, 764, 765, 769, 771, 868, 870, 871, 875, 877, 996, 999, 1001, 1190, 1191
PIKKs-sites
410, 1200, 1410

E
DAPI/Treacle-Katushka Ph-mut
HIGH expression
5 µm
Drops/cell
**
wt
Ph-mut

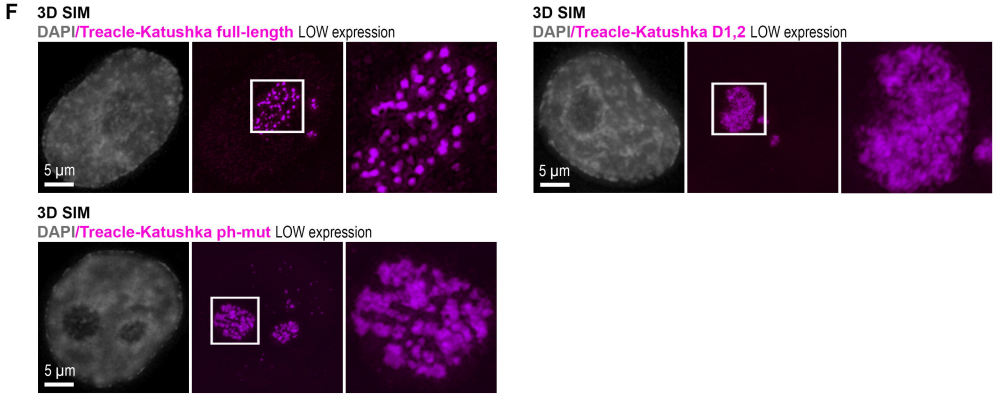
F
3D SIM
DAPI/Treacle-Katushka full-length LOW expression
5 µm
3D SIM
DAPI/Treacle-Katushka D1,2 LOW expression
5 µm
3D SIM
DAPI/Treacle-Katushka ph-mut LOW expression
5 µm

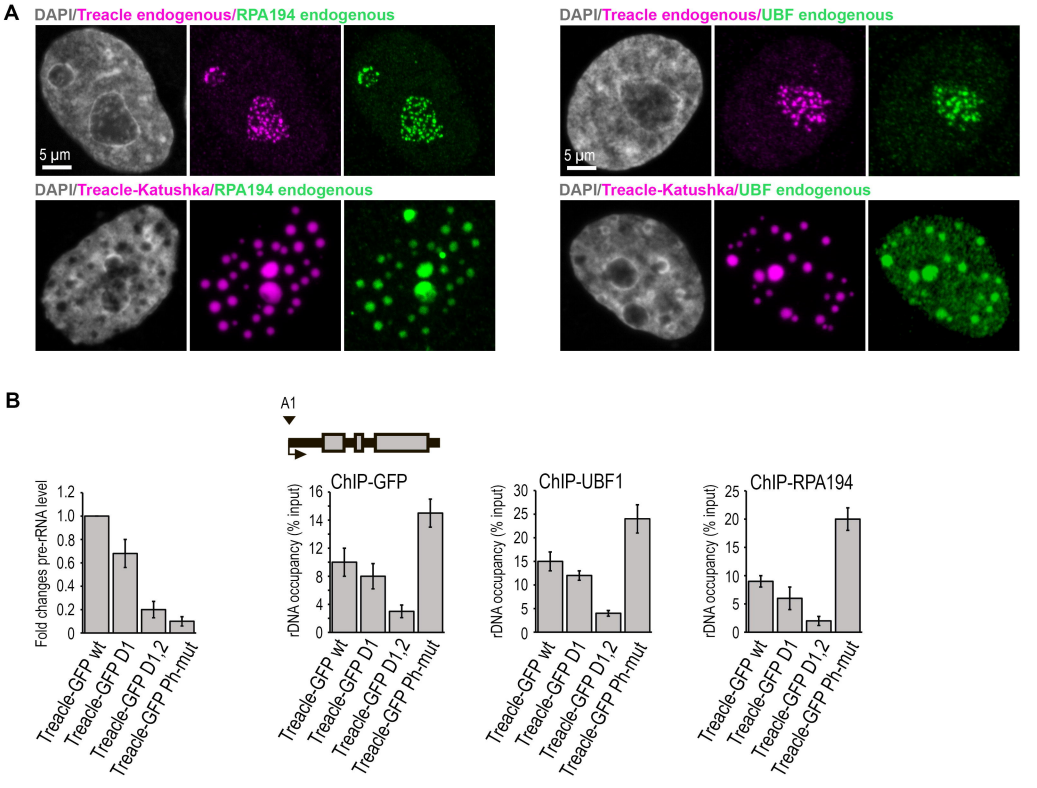
A
DAPI/Treacle endogenous/RPA194 endogenous
5 µm
DAPI/Treacle endogenous/UBF endogenous
5 µm
DAPI/Treacle-Katushka/RPA194 endogenous
DAPI/Treacle-Katushka/UBF endogenous
B
A1
Fold changes pre-rRNA level
1.2
1.0
0.8
0.6
0.4
0.2
0
Treacle-GFP wt
Treacle-GFP D1
Treacle-GFP D1,2
Treacle-GFP Ph-mut
ChIP-GFP
rDNA occupancy (% input)
16
14
12
10
8
4
0
ChIP-UBF1
30
25
20
15
10
5
0
ChIP-RPA194
25
20
15
10
5
0

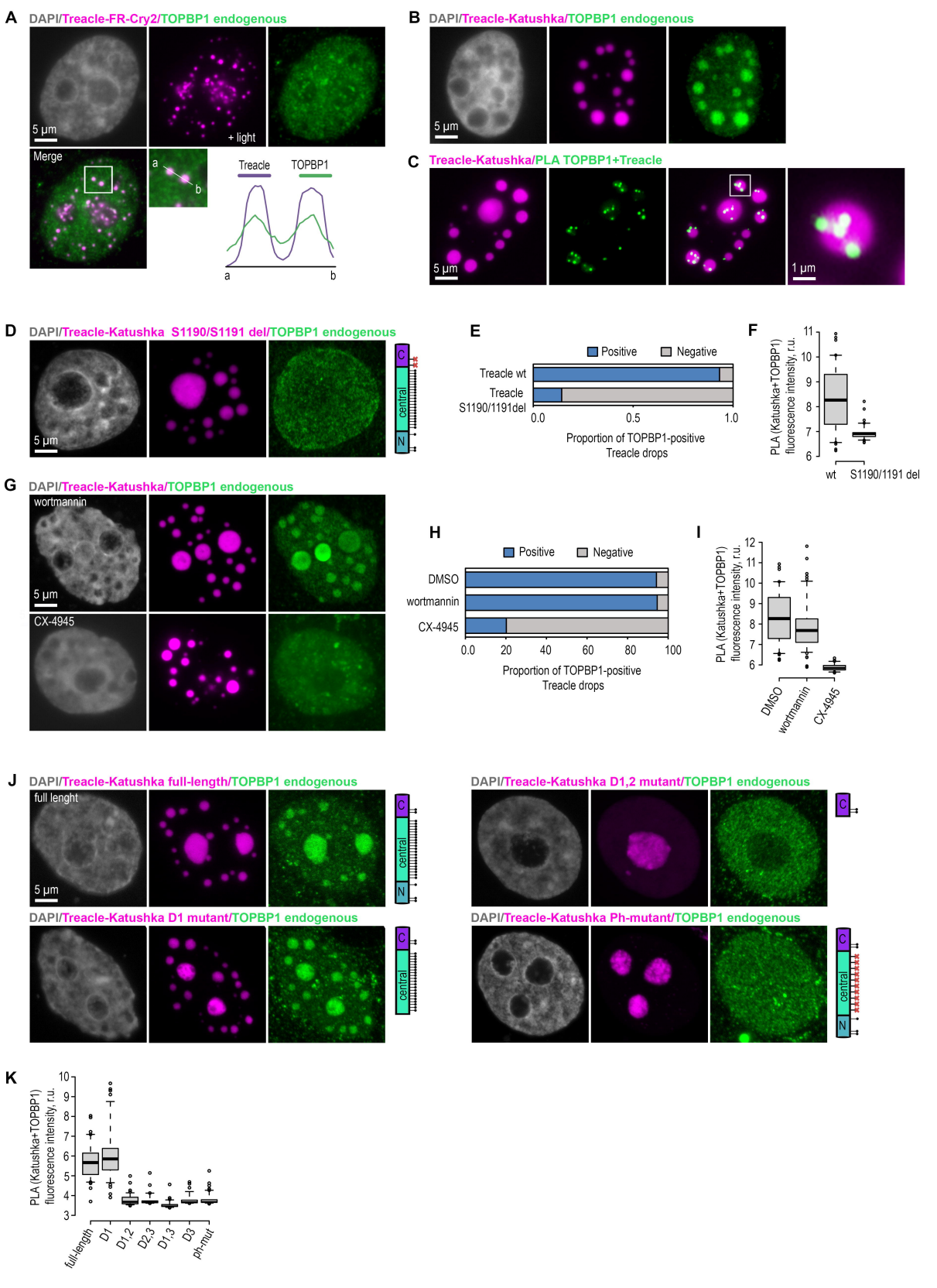
A
DAPI/Treacle-FR-Cry2/TOPBP1 endogenous
5 µm
+ light
Merge
a
b
Treacle
TOPBP1
B
DAPI/Treacle-Katushka/TOPBP1 endogenous
5 µm
C
Treacle-Katushka/PLA TOPBP1+Treacle
5 µm
1 µm
D
DAPI/Treacle-Katushka S1190/S1191 del/TOPBP1 endogenous
5 µm
C
central
N
E
Positive
Negative
Treacle wt
Treacle S1190/1191del
0.0
0.5
1.0
Proportion of TOPBP1-positive Treacle drops
F
PLA (Katushka+TOPBP1) fluorescence intensity, r.u.
wt
S1190/1191 del
G
DAPI/Treacle-Katushka/TOPBP1 endogenous
wortmannin
5 µm
CX-4945
H
Positive
Negative
DMSO
wortmannin
CX-4945
0.0
20
40
60
80
100
Proportion of TOPBP1-positive Treacle drops
I
PLA (Katushka+TOPBP1) fluorescence intensity, r.u.
DMSO
wortmannin
CX-4945
J
DAPI/Treacle-Katushka full-length/TOPBP1 endogenous
full lenght
5 µm
C
central
N
DAPI/Treacle-Katushka D1,2 mutant/TOPBP1 endogenous
C
DAPI/Treacle-Katushka D1 mutant/TOPBP1 endogenous
C
central
DAPI/Treacle-Katushka Ph-mutant/TOPBP1 endogenous
C
central
N
K
PLA (Katushka+TOPBP1) fluorescence intensity, r.u.
full-length
D1
D1,2
D2,3
D1,3
D3
ph-mut

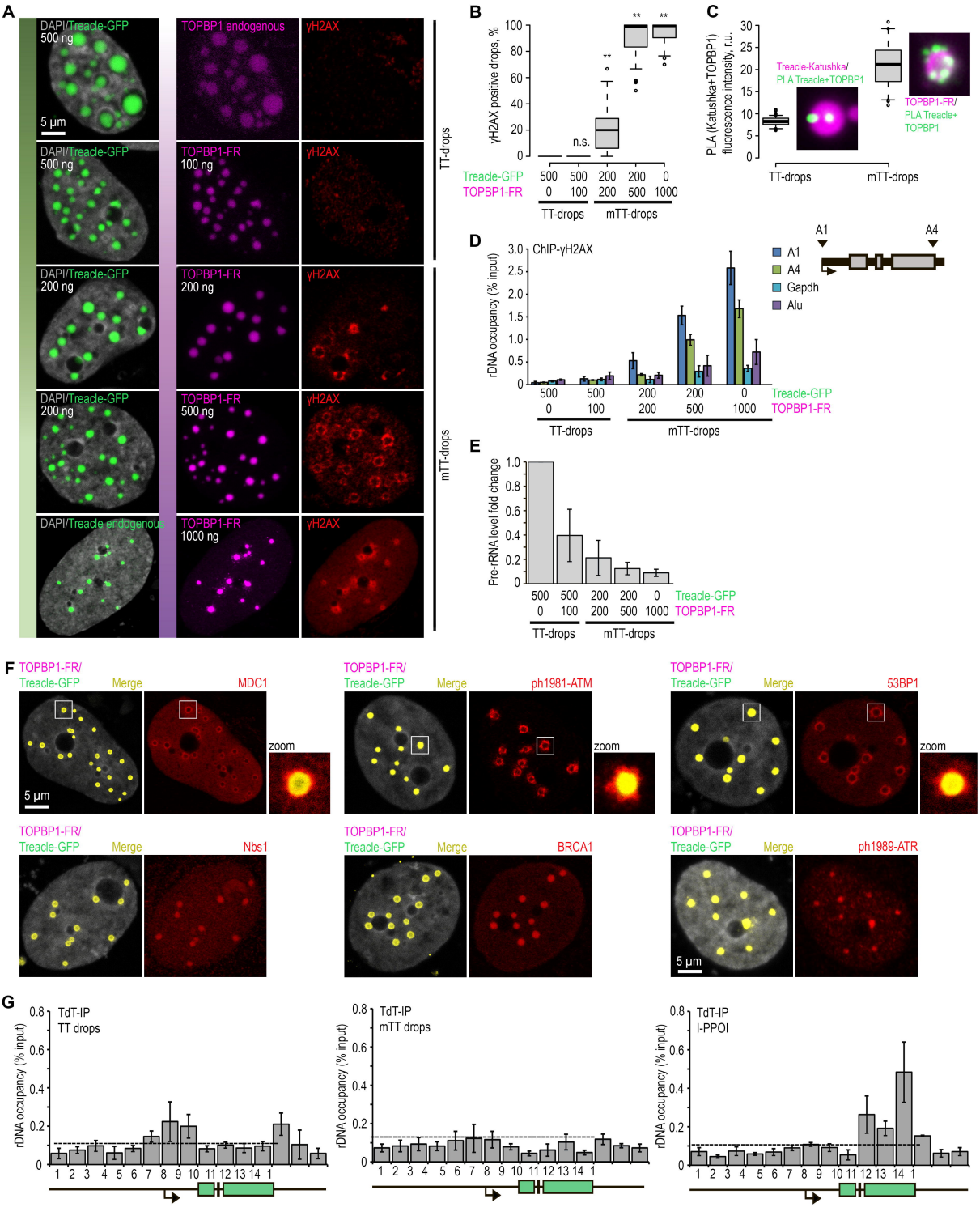
A
DAPI/Treacle-GFP 500 ng
5 µm
TOPBP1 endogenous
γH2AX
DAPI/Treacle-GFP 500 ng
TOPBP1-FR 100 ng
γH2AX
TT-drops
DAPI/Treacle-GFP 200 ng
TOPBP1-FR 200 ng
γH2AX
DAPI/Treacle-GFP 200 ng
TOPBP1-FR 500 ng
γH2AX
DAPI/Treacle endogenous
TOPBP1-FR 1000 ng
γH2AX
mTT-drops
B
γH2AX positive drops, %
n.s.
**
Treacle-GFP 500 500 200 200 0
TOPBP1-FR 0 100 200 500 1000
TT-drops
mTT-drops
C
PLA (Katushka+TOPBP1) fluorescence intensity, r.u.
Treacle-Katushka/ PLA Treacle+TOPBP1
TOPBP1-FR/ PLA Treacle+ TOPBP1
TT-drops
mTT-drops
D
ChIP-γH2AX
rDNA occupancy (% input)
A1
A4
Gapdh
Alu
Treacle-GFP 500 500 200 200 0
TOPBP1-FR 0 100 200 500 1000
TT-drops
mTT-drops
E
Pre-rRNA level fold change
Treacle-GFP 500 500 200 200 0
TOPBP1-FR 0 100 200 500 1000
TT-drops
mTT-drops
F
TOPBP1-FR/ Treacle-GFP
Merge
MDC1
ph1981-ATM
53BP1
Nbs1
BRCA1
ph1989-ATR
zoom
5 µm
G
TdT-IP TT drops
TdT-IP mTT drops
TdT-IP I-PPOI
rDNA occupancy (% input)

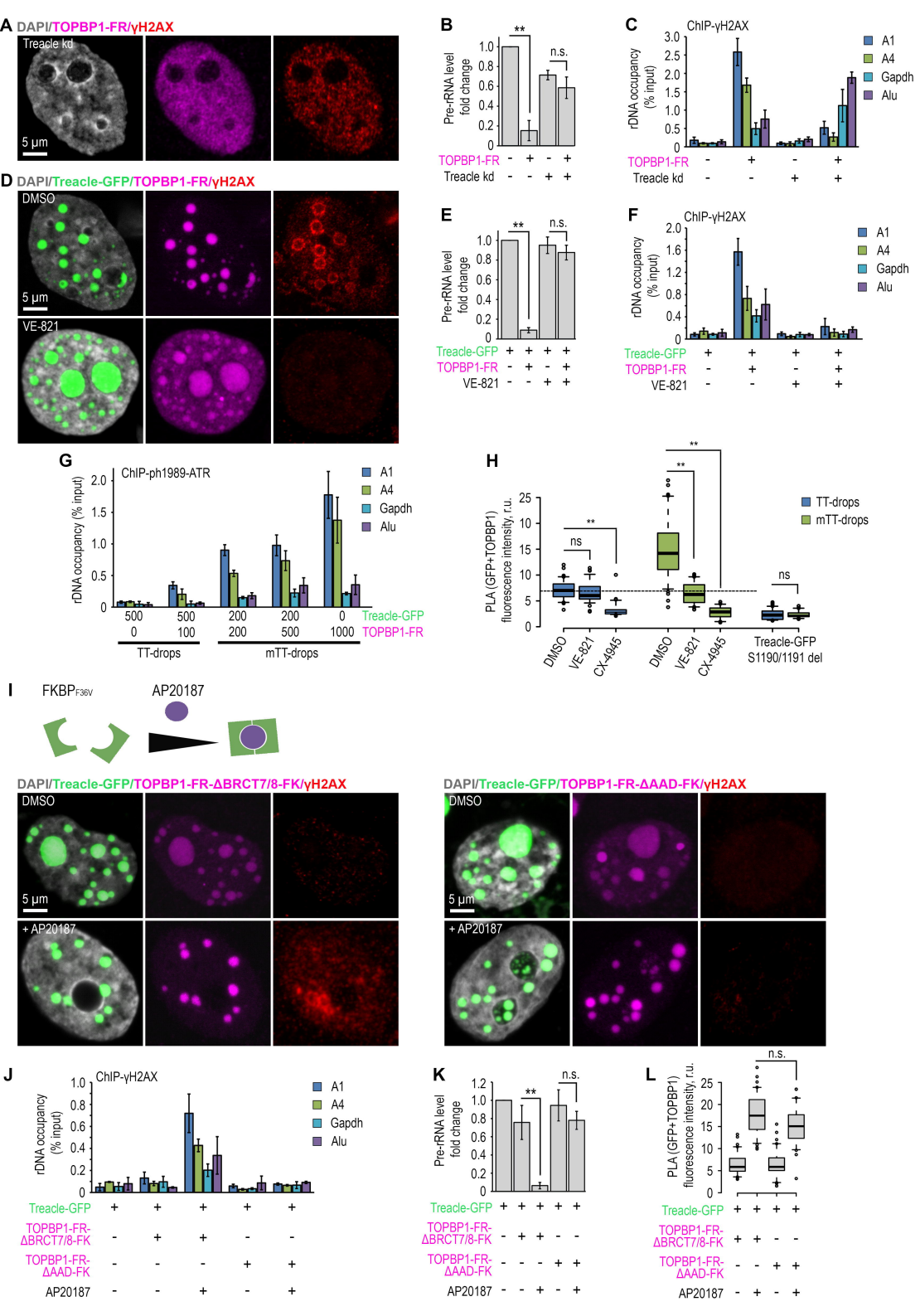
A
DAPI/TOPBP1-FR/γH2AX
Treacle kd
5 µm
B
Pre-rRNA level fold change
**
n.s.
TOPBP1-FR
Treacle kd
C
ChIP-γH2AX
rDNA occupancy (% input)
A1
A4
Gapdh
Alu
TOPBP1-FR
Treacle kd
D
DAPI/Treacle-GFP/TOPBP1-FR/γH2AX
DMSO
VE-821
5 µm
E
Pre-rRNA level fold change
Treacle-GFP
TOPBP1-FR
VE-821
F
ChIP-γH2AX
rDNA occupancy (% input)
G
ChIP-ph1989-ATR
rDNA occupancy (% input)
TT-drops
mTT-drops
Treacle-GFP
TOPBP1-FR
H
PLA (GFP+TOPBP1) fluorescence intensity, r.u.
TT-drops
mTT-drops
ns
DMSO
VE-821
CX-4945
Treacle-GFP S1190/1191 del
I
FKBPF36V
AP20187
DAPI/Treacle-GFP/TOPBP1-FR-ΔBRCT7/8-FK/γH2AX
DMSO
+ AP20187
5 µm
DAPI/Treacle-GFP/TOPBP1-FR-ΔAAD-FK/γH2AX
DMSO
+ AP20187
5 µm
J
ChIP-γH2AX
rDNA occupancy (% input)
A1
A4
Gapdh
Alu
Treacle-GFP
TOPBP1-FR-ΔBRCT7/8-FK
TOPBP1-FR-ΔAAD-FK
AP20187
K
Pre-rRNA level fold change
**
n.s.
Treacle-GFP
TOPBP1-FR-ΔBRCT7/8-FK
TOPBP1-FR-ΔAAD-FK
AP20187
L
PLA (GFP+TOPBP1) fluorescence intensity, r.u.
n.s.
Treacle-GFP
TOPBP1-FR-ΔBRCT7/8-FK
TOPBP1-FR-ΔAAD-FK
AP20187

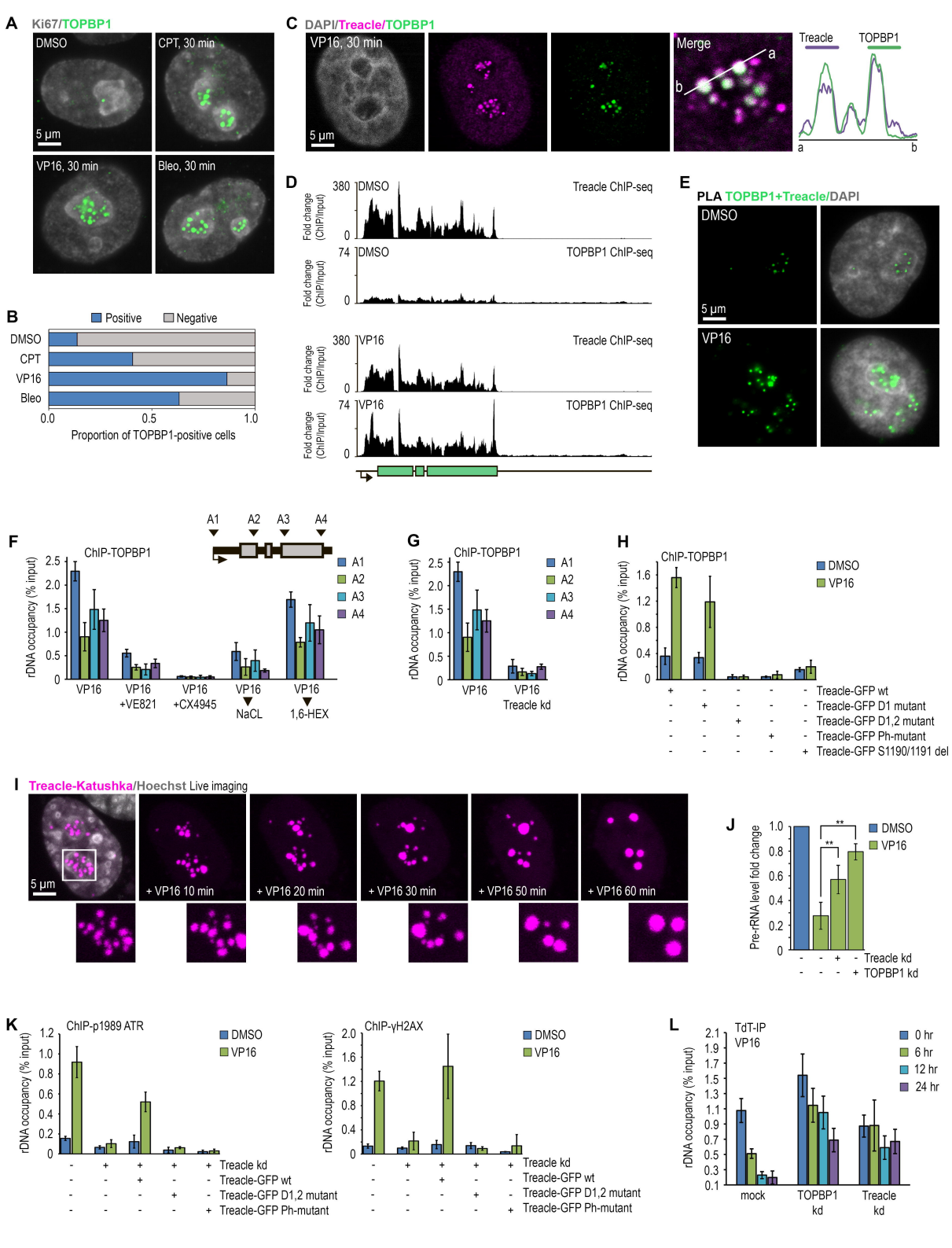
A
Ki67/TOPBP1
DMSO
CPT, 30 min
VP16, 30 min
Bleo, 30 min
5 µm
B
Positive
Negative
DMSO
CPT
VP16
Bleo
0.0
0.5
1.0
Proportion of TOPBP1-positive cells
C
DAPI/Treacle/TOPBP1
VP16, 30 min
5 µm
Merge
a
b
Treacle
TOPBP1
D
Treacle ChIP-seq
TOPBP1 ChIP-seq
Fold change (ChIP/Input)
380
74
0
DMSO
VP16
E
PLA TOPBP1+Treacle/DAPI
DMSO
VP16
5 µm
F
ChIP-TOPBP1
rDNA occupancy (% input)
A1
A2
A3
A4
VP16
VP16 +VE821
VP16 +CX4945
VP16 NaCL
VP16 1,6-HEX
G
ChIP-TOPBP1
VP16
VP16 Treacle kd
H
ChIP-TOPBP1
DMSO
VP16
Treacle-GFP wt
Treacle-GFP D1 mutant
Treacle-GFP D1,2 mutant
Treacle-GFP Ph-mutant
Treacle-GFP S1190/1191 del
I
Treacle-Katushka/Hoechst Live imaging
5 µm
+ VP16 10 min
+ VP16 20 min
+ VP16 30 min
+ VP16 50 min
+ VP16 60 min
J
Pre-rRNA level fold change
DMSO
VP16
Treacle kd
TOPBP1 kd
K
ChIP-p1989 ATR
ChIP-γH2AX
DMSO
VP16
Treacle kd
Treacle-GFP wt
Treacle-GFP D1,2 mutant
Treacle-GFP Ph-mutant
L
TdT-IP
VP16
0 hr
6 hr
12 hr
24 hr
mock
TOPBP1 kd
Treacle kd